EMERGING ADVANCED TECHNOLOGIES TO ASSESS RELIABILITY OF INDUSTRIAL STEAM TURBINE BLADE DESIGN

by

Murari Singh

Consulting Engineer/Probabilistic Lifing Leader

GE Oil & Gas

Bethlehem, Pennsylvania

and

Michael J. Drosjack

Senior Principal, Rotating Equipment Department

Shell Global Solutions (US) Inc.

Houston, Texas

Murari P. Singh is Consulting Engineer/ Probabilistic Lifing Leader of GE Oil & Gas, in Bethlehem, Pennsylvania, for all products in the Chief Engineers' Office. He has been involved in the design, development, and analysis of industrial turbomachinery for more than 30 years at Turbodyne Corporation, Dresser Industries, Dresser Rand Company, and, most recently, with Safe Technical Solutions Inc., where he served as Director of Engineering Technology. Dr. Singh has extensive knowledge and experience with fatigue and fracture mechanics, stress and vibration of structures, reliability, life analysis, and probabilistic analysis. His practical application experience includes a variety of rotating equipment including warm gas and FCC expanders, steam turbines, and centrifugal compressors.

Dr. Singh holds B.S., M.S., and Ph.D. degrees, and he has authored more than 30 technical papers on a variety of topics related to turbomachinery. Notably, Dr. Singh developed the widely used SAFE diagram for reliability evaluation of turbine blades.

Michael J. Drosjack is a Senior Principal in the Rotating Equipment Department at Shell Global Solutions (US) Inc., in Houston, Texas. He is responsible for providing technical support for rotating and reciprocating machinery to Shell and Shell affiliated companies worldwide, as well as commercial customers. Since joining Shell in 1975, he has had assignments on projects involving specification, evaluation, installation, and startup of machinery along with extensive field troubleshooting, particularly in the area of vibration measurement, vibration analysis, and rotordynamics.

Dr. Drosjack received his B.S. degree (Mechanical Engineering, 1970) from Carnegie-Mellon University, and his M.S. (1971) and Ph.D. (1974) degrees (Mechanical Engineering) from The Ohio State University. He is a member of ASME, the Vibration Institute, the Machinery Subcommittee of the Ethylene Products Committee, participates in API task forces, and has been a speaker and panelist for NPRA. He has been a Turbomachinery Symposium Advisory Committee member since 1986.

ABSTRACT

New industrial processes sometimes require equipment that either has not yet been applied to the new use or even a completely new design. In some situations, established design criteria that have resulted in reliable equipment in past years may no longer be adequate. Therefore, one needs to turn to new technologies that have been developed by researchers.

This presentation will review the state of promising technologies that may be or have recently been applied in estimating the reliability of steam turbine blades. Specifically, the discussion will detail the currently applied design tools including topics such as bladed disk vibration, mistuning of bladed disks, computational fluid dynamics (CFD) and the damping concept. An assessment of the useful life of a blade will be calculated for the high cycle fatigue under load. However, it should be realized that there would always be uncertainty associated with any design decision. Therefore, a probabilistic concept will be discussed and employed to quantify the risk of the proposed design as a means to more accurately evaluate this life. Examples will be employed to demonstrate the technology.

INTRODUCTION

Structural integrity of all rotating components is the key for successful operation of any turbomachinery. The integrity depends on the successful resistance of the machine parts to the steady and alternating stresses imposed on them. The challenge with rotating equipment is often more severe due to the significance of the alternating loads that must be carried to satisfy their purpose. This is less of a factor in stationary equipment where static loading more commonly predominates. And, static loading is generally more amenable to accurate prediction. Srinivasan (1997) in his scholarly paper described the state of the art of the technology and the many gaps that exist with regard to gas turbine engines applied to aviation. Many of the advances mentioned in the paper have been applied to steam turbine design.

One of the major classes of rotating machinery is mechanical drive steam turbine, i.e., steam turbines that drive pumps and/or compressors. These steam turbines are differentiated from generator drives in that they operate at variable speeds. Steam turbines may operate from 1 to 5 horsepower up to several hundred thousand horsepower; they may operate with steam that ranges from vacuum to thousands of pounds per square inch; and, blade tip speeds can exceed the force of the most severe hurricanes (a

large, last blade row with an 8 foot tip to tip diameter operating at 3600 rpm will experience tip speeds in excess of 1000 mph).

Static stress is primarily the result of steam bending and centrifugal loads. Alternating stresses are imposed due to the vibration of the parts in question, e.g., blades and disks. If the combined loads become too large, vibration-induced fatigue of the rotor blades or disks is a major concern. In addition to the imposed loads, these forces are also subject to resonant amplification caused by coincidence with natural frequencies. To put the scope of this problem into context, one must realize that there may be thousands of blades in a steam turbine. There may be 10 to 20 rows of different blade designs and the possibility that each blade row having different dynamic characteristics.

Steam turbines have been in operation for more than 100 years and have always faced this problem. As may be imagined, the technology in engineering and physics to support these designs has grown dramatically over that time. Tools have been enhanced and technological developments incorporated.

The current state of design, as may be represented in the American Petroleum Institute (API) standards for this class of machinery, sets a life of 30 years for all components. In many cases, this translates into a design requirement for infinite life. This may exceed the needs of a specific installation. This requirement may be driven by the actual desire for infinite life, limitations in analysis techniques and tools that have existed over the years, and/or an incomplete understanding of the tools that have appeared in the recent past and are currently fully or partially available.

The current reality dictates that in the quest for improving efficiency, higher stage loading, higher pressure, reduced axial gaps, and larger diameter disk designs have been pushed for higher speed, higher temperature, etc. Failures typically drive the requirement for development of enhanced design tools and methodology. The evolution of new operating requirements requires machines to be designed outside the existing experience envelope. Thus utilization of techniques such as three dimensional stress analysis, bladed disk vibration analysis, better characterization of material behavior, and better understanding of aerodynamics becomes more of a requirement.

This tutorial will discuss the tools and techniques currently applied as *"the standard"* in the industry today. This case is described as *deterministic* analysis to reach a single acceptable value. It will then go further into the potential application of tools (many available and others still under development) in the arena of *probabilistic* analysis. This method of analysis may optimize the design to more exactly meet the requirements of the service rather than always exceed it through the application of a substantial safety margin. This evaluation requires an understanding and acceptance of a finite *risk* of failure. The opportunity that presents itself can yield economic optimization. While currently in limited use, it is a fact is that these advanced tools and techniques are being continually improved and may become the current reality over time.

For example, one may need as the ultimate design state, a 90 percent likelihood of eight years blade life since the turbine is planned to be replaced at that time interval. One might be sacrificing a much improved design basis cost, delivery, efficiency, size, or weight to those requirements to get an infinite life design.

For those who might say that this is impossible, too far into the future, inconceivable, the authors would ask them to remember the late 1800s and early 1900s when the British Society commissioned a study that concluded that "it was not physically possible for a rotor to operate at or above its first rotational resonant speed." This learned conclusion was published some short time after Gustav de Laval built and operated a steam turbine that indeed operated above its first rotational resonant speed.

DISCUSSION OF CURRENT TECHNOLOGY

A common cause of vibration-related failure in steam turbine blading is resonant excitation of the blading occurring at an integral order, i.e., multiples of the rotational speed, nozzle passing frequency, and multiples of nozzle passing frequency. The associated mode of failure is high cycle fatigue. A primary feature of resonance is that dynamic stress amplitude rises as the exciting frequency approaches the resonant speed. The response decreases after passing through the resonant speed. Hence, it is necessary to identify resonant frequencies of the system.

In order to calculate the resonance characteristics of blades one needs to deal with the following key issues (not all inclusive):

- Unsteady aerodynamics over a wide variety of flow conditions that may exist within the operating range,
- Structural vibration characteristics, i.e., frequencies and associated mode shapes within the operating range,
- Damping in the system (structural as well as aerodynamic),
- Estimate of material properties (fatigue properties, yield strength, ultimate strength, modulus of elasticity, etc.) at the temperature in the operating range.

Each of these issues may require a separate technical discipline to support an evaluation. In the last few decades, significant advances have been made in several of these even though additional analytical and test development is still needed. Utilization of the current state-of-the-art technologies and tools will no doubt provide a better evaluation of the issues resulting in more accurate, optimal designs.

Unsteady aerodynamic analysis can produce two necessary pieces of data: aerodynamic damping and the magnitude of the pressure acting on the blade (pressure profile due to flow variation). During each revolution each blade experiences variation in pressure or force. It will feel the same force in the subsequent revolutions. Each blade experiences a periodic force with a time lag with respect to its neighbor. These aerodynamic forces depend on blade geometry (profile, stagger angle, angle of incidence), cascade solidity, and flow conditions (i.e., subsonic, transonic, and supersonic). It is more complex when shock or flow separation occurs.

The blade structural dynamic analysis must consider an assembly of blades and the disk as a system. The characterization includes natural frequencies in the operating range, associated mode shapes, and damping. These are the required input for estimating the forced response of the bladed disk assembly. Since the blades vibrate in a flow medium, an interdisciplinary approach that includes structural dynamics and unsteady aerodynamic analysis is necessary.

The amplitude of the dynamic stress is proportional to the damping. Damping is provided by a material's internal resistance as well as by the flow medium (aerodynamic damping). More is known about material damping but aerodynamic damping depends on the characteristics of the flow. For example a blade will experience more resistance to vibration in a dense gas than a less dense gas. It is also seen that a tall blade will experience more damping due to a larger amplitude of vibration than a shorter blade having a smaller amplitude of vibration, i.e., damping can be wildly nonlinear.

Even after a comprehensive design analysis and prudent manufacturing, blades have failed in service and even sometimes during demonstration tests. It should be realized that blades of supposedly identical design have failed after different times in operation. This is not only true for blades having supposedly the same design but also for identical blades in different machines.

Current and former successful results have been achieved by applying experienced based rules and limits. These rules and limits can cause designs that may seem to run out of space (the limits set design boundaries that may not be analytically sound). This may impose overdesign requirements that may damage the economic viability of equipment designs cascading to projects.

The next section will review in detail the pertinent technologies that have been applied in the design and evaluation of the reliability of steam turbine blades. Discussions include bladed disk vibration, mistuning of bladed disks, computational fluid dynamics (CFD),

and the damping concept. The assessment of the useful blade life is discussed with respect to damage from high cycle fatigue. As there is always a risk associated with any design decision, a probabilistic concept will be presented that permits a quantification of the risk of a proposed design. The potential to apply probabilistic analysis to extend design capabilities is presented at the end of this discussion to demonstrate how this is all pulled together with the probabilistic analysis.

Bladed Disk Vibration

The last five decades have seen phenomenal theoretical development toward the understanding of the vibrational behavior of bladed disk systems. A very significant enabler has been the growth in the availability of ever more powerful computers.

In the simplest analysis, a spring mass lumped model was used to study the vibrational behavior of a blade. This early approximation and method led to the concept of resonance. It showed that the coincidence of frequencies (forcing frequency and natural frequency) produced the largest amplitude of vibrational response. At the next level of complexity, the behavior of a single cantilevered beam was studied by considering it as a continuum rather than lumped. Theories of bending and vibration of a beam were utilized. Later researchers realized that, in the case of banded (shrouded) blades, there existed more natural modes and natural frequencies than those estimated from a single beam model. This is due to the existence of coupling among the blades of a packet through the shroud band. The study (Weaver and Prohl, 1956) of this phenomenon identified the existence of many modes and frequencies a packet of blades not detected by a single blade analysis. Packets of blades are mounted on a disk and packets are coupled to each other through the disk. Analytical results as well as test data show that many modes and frequencies are influenced by the stiffness of the disk. These additional modes are not calculable through the analysis of a single packet of cantilevered blades and require the next level of complexity.

Single Degree of Freedom (SDOF) System

The analysis of a spring mass system (Figure 1) provides the basis for understanding the vibration characteristics of a mechanical system. Application of Newton's Third Law of Motion yields the equation of motion for the above case:
where:

$$m\,a + c\,v + k\,x = F(t).\cos(A) \qquad (1)$$

m is the mass
a is the acceleration of the mass, m
c is the viscous damping
v is the velocity of the mass
k is the stiffness
x is the vertical displacement
$F(t) = F_0 \sin(\omega t)$ is the time dependent force, and angle A defines the direction of force from the vertical direction.

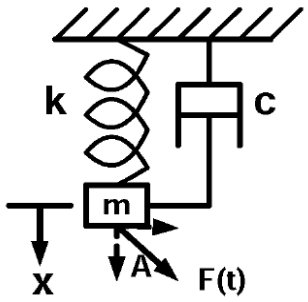

$$m.a + c.v + k.x = F(t).\cos(A)$$

Figure 1. Single Spring-Mass-Damper System.

Assuming a harmonic solution for the displacement, x(t), to be:

$$x(t) = C_0 \sin(\omega t + \phi) \qquad (2)$$

The absolute magnitude of the response magnifier is expressed as:

$$\text{Abs}\,(C_0 k / F_0) = \cos(A) / \left((1-r^2)^2 + (2\zeta r)^2\right)^{1/2} \qquad (3)$$

where:
r = ω/ω_n
ω_n = $(k/m)^{1/2}$
ζ = $c/(2(km)^{1/2})$
C_0 = Amplitude of vibration
F_0/k = Displacement if the magnitude of an applied steady state force is equal to F_0

Singh and Schiffer (1982), Singh and Ewins (1988), Singh, et al., (1988), and Singh and Vargo (1989) discussed the resonance of a circular symmetric structure and pointed out that resonance can be viewed as a state in which the energy built up in the system due to applied forces attains a maximum value. Thus, in the state of resonance, the magnitude of the response (stress, displacement) of the system also attains its maximum value and the system's resistance to the exciting forces is minimum (Figures 2 and 3). ζ represents the percent of critical damping. At frequency ratio r = 1, the exciting frequency equals the natural frequency and the magnifier is maximized.

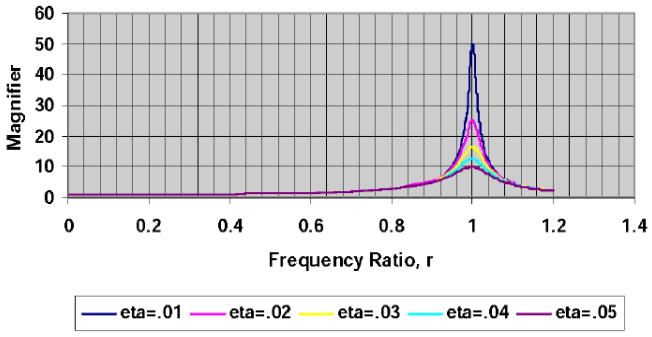

Figure 2. Absolute Value of Magnifier Versus Frequency Ratio.

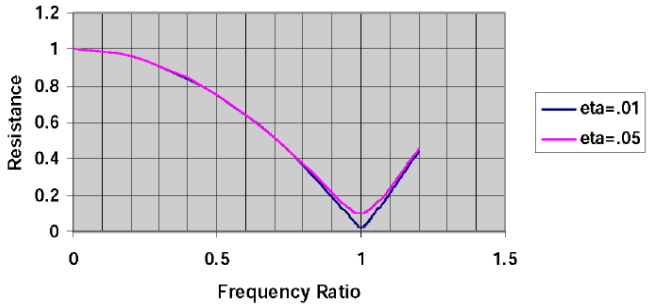

Figure 3. Resistance Versus Frequency Ratio.

Figure 4 shows the variation of the peak response of the mass as a function of the direction of the force. The degree of freedom of the spring-mass-damper system is the displacement in the vertical direction, i.e., the mass can move only up and down. The system will respond only to the vertical component of the force, F. The response is greatest when the force acts in the vertical direction (angle, A equal to zero) and the response is zero when the vertical component of the force is zero (angle A equals 90 degrees). The mode shape (motion pattern in the vertical direction) matches only with the vertical component of the force.

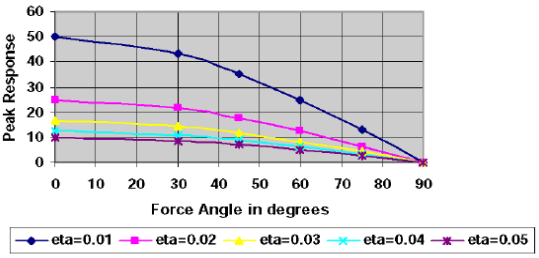

Figure 4. Peak Response Versus Angle of the Force.

The assumptions and key points that form the basis for understanding the behavior of a bladed disk are:

- The displaced form of the blades in a packet should be similar to the displaced form exhibited by a single blade in a similar mode of vibration.
- A disk should exhibit similar behavior with or without blades.
- The displaced form of the cantilevered packet (as a system) is expected to be similar during the vibration of a bladed packeted disk.

Single Cantilevered Blade

It is instructive to examine the expected natural modes for a single cantilevered blade. The expected shapes of the first three modes are shown in Figure 5. The end of the blade attached to ground has zero displacement, a condition for being joined to ground. For the first mode all the points of the blade at any given time in its one cycle of vibration move in the same direction. For the second mode there is a point of zero displacement (a node) along the blade. This means that during vibration, locations on one side of the node move in the opposite direction to the locations on the other side of the node. This is called a phase change. The zero displacement point, of course, has zero velocity. The third mode changes phase two times. Similarly the fourth mode should change phase three times and so on.

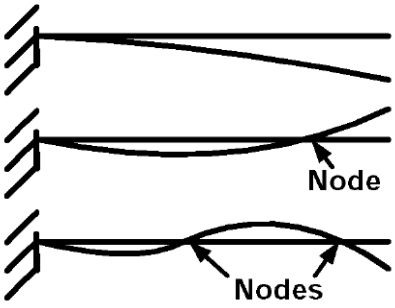

Figure 5. Mode Shapes of a Cantilevered Beam.

Packet of Blades

A packet is a collection of blades that are connected together at the tip by a band of metal called a shroud. Due to the coupling through the shroud, a packet exhibits many more modes than a single blade. The number of these modes depends on the number of blades in the packet (refer to Figure 6 for a description of the modes of a packet with different numbers of blades). The displacement in the plane of the disk is referred to as tangential and that out of the plane of the disk is called axial. It is assumed that any torsional vibration of the blade is coupled with the higher order axial vibration.

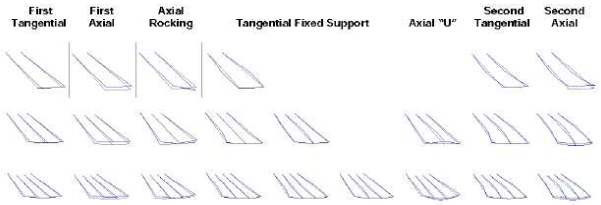

Figure 6. Some Mode Shapes of a Packet of Blades.

Some key observations are noted from analysis of a packet of two blades for simplicity:

- The displaced form of the blades in a packet should be analogous to the displaced form exhibited by a single blade in a similar mode of vibration.
- There are two modes in which blades either move in phase or out of phase as exhibited in the first tangential and tangential fixed support modes. The displacement of blades in the first tangential and tangential fixed support modes are considered similar.
- The observations made are also true for axial bending. The blades move in unison in the first axial mode while in axial rocking they move opposite to each other.
- Statistically, if there are two masses, they will move two ways in relation to each other. First they move in phase and second, they move out of phase.
- The implication is that the number of modes that will exhibit the primary displaced shape will be equal to the number of blades. This is also evident in Figure 6 for packets with three blades and the packets with four blades.

Individual Disks

For each natural frequency ω_{mn} there are two corresponding natural modes, except for m = 0, where m is the number of nodal diameters and n is the number of nodal circles. In case when m is not equal to zero, mode is degenerate. For a vibrating disk, there are two distinct locations where displacements are zero. These locations form either radial lines or circles. Two radial lines are considered to be a diameter for describing a mode. These are named nodal diameters and the other is named nodal circles. For an axisymmetric structure, the displacement has a sine wave form. These are shown in Figure 7.

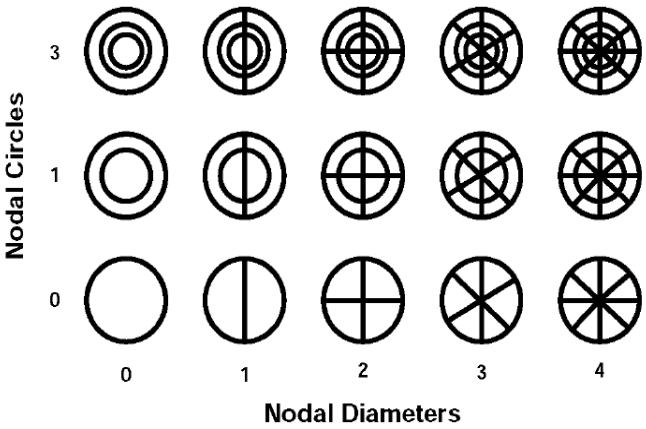

Figure 7. Modes of Vibrating Disks.

ANALYSIS OF A BLADED DISK SYSTEM

Free Standing (Blades With or Without a Shroud but Not Connected to Each Other)

The behavior of the bladed disks as one system is described without delving into complex mathematical expressions. It should be noted that there is a coupling between the blades in the packet through the shroud and there is also a coupling between packets through the disk.

Turbines may be designed and manufactured with some stages in which blades are not connected through their shrouds. Two types of construction are prevalent. In one design, the shroud is used as a cover for individual blades but not for connecting to the next blade. The second type of construction does not have any

shroud. If the same disk is used to mount these two types of blades, the natural frequencies are expected to be different but the mode shapes will be similar. When blades are mounted on a disk, their natural frequencies are influenced by the stiffness of the disk just as the frequencies of a packet were influenced by the shroud's stiffness. Statistically, the total number of modes displaying one type of blade bending mode will be equal to the number of blades. In vibration of the first mode, all blades move in the same direction at any time in the vibration cycle, i.e., they move in phase. This mode is called the zero nodal diameter or umbrella mode. The amplitude of vibration of each blade will be identical at any time.

Figure 8 is a plot of the displacements of the tip of the blades. The displacements of the rim of the disk are also plotted. In this example, there are 120 blades on the disk. Even though this is a mode shape of a packeted bladed disk, it shows the typical behavior of a bladed disk with or without a shroud. This particular mode can be described by the function sin(3θ) and contains three full sine waves. It has been explained earlier that the modes of a disk can be described by a sine function. There is an accompanying mode at the same frequency that can be represented by a cosine function.

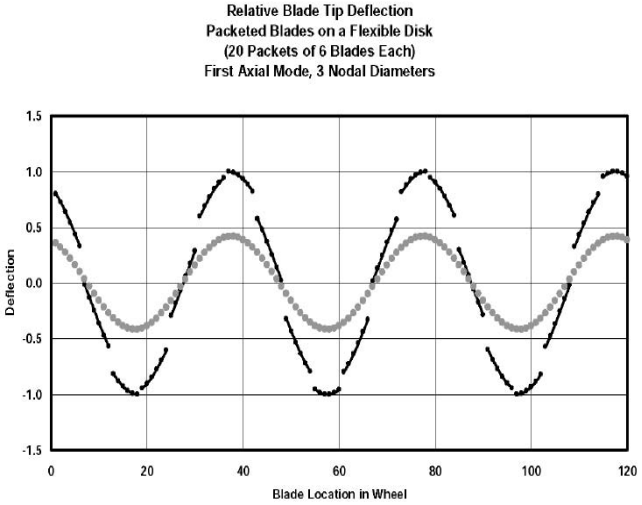

Figure 8. Three Nodal Diameter Mode.

It is customary to use the nomenclature of *nodal diameter* to describe the modes of a bladed disk (Figure 7). For example a mode with one sine wave is mathematically described by the function sin2 and is named 1ND (one nodal diameter). Half the number of blades move in one direction, and the other half move in the opposite direction—there is one phase change in the displacement. The pattern of displacement is similar to a single cosine or a single sine wave.

The natural frequency is plotted on the y-axis corresponding to the mode shape (ND) that is plotted on the x-axis (Figure 9). The disk behavior is similar to the curve as shown. The frequency will increase as the order nodal diameter mode order increases. Natural frequencies have the same magnitude for cantilevered blades. The reason for this is that the base of the blade is anchored to ground, i.e., the base has infinite stiffness. For blades mounted on a very stiff disk, their characteristics are expected to be similar. This assumption is nearly realized when the vibration of blades on a disk is considered in the tangential direction. When a blade is mounted on the disk the resultant behavior is as shown. In low order nodal diameter modes, the disk seems to control the behavior, while at higher order modes, the blade seems to control the behavior. There is a transition zone where the relative stiffness between the disk and blade seems to play the controlling role.

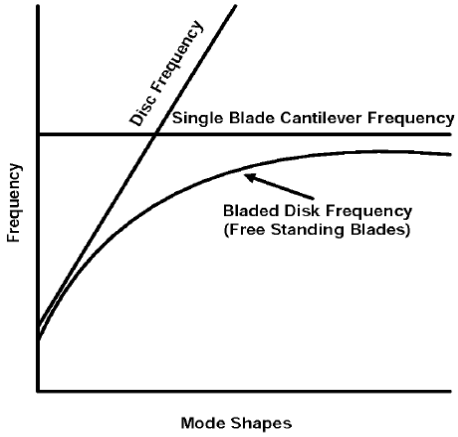

Figure 9. Representative Behavior of Disk Alone, Blade Alone, and Bladed Disk.

Packeted Bladed Disk

Singh and Schiffer (1982) reported a study of the vibrational characteristics of a packeted bladed disk (during tangential vibration mode). Some salient features of the study are worth mentioning and some key points of the results will be discussed here. Results of a finite element analysis of a turbine stage containing 90 blades are shown. This stage contained 15 packets of six blades each mounted on the disk. The results of a cantilevered packet of blades in the tangential direction are tabulated. The natural frequencies of the first six tangential modes are listed in Table 1. A list of frequencies with associated mode shapes for the packeted blade disk analysis is reproduced in Table 2.

Table 1. Frequencies and Mode Shapes for a Cantilevered Packet.

Number of Modes	Mode Shapes	Natural Frequency, hz
1	First Tangential	2612.0
2	Tang. Fixed Support-1	10150.0
3	Tang. Fixed Support-1	11678.0
4	Tang. Fixed Support-1	11948.0
5	Tang. Fixed Support-1	12030.0
6	Tang. Fixed Support-1	12049.0

Table 2. Packeted Bladed Disk Frequencies and Mode Shapes.

	Packeted Bladed Disc		Single Packet		Packeted Bladed Disc		Single Packet
Number of Modes	Mode Shapes, ND	Natural frequencies, hz	Mode Shapes and Natural Frequencies, hz	Number of Modes	Mode Shapes, ND	Natural frequencies, hz	Mode Shapes and Natural Frequencies, hz
1	0	1338.86		46	23	11913.05	Tang. Fixed Support-3, 11948.0
2	1	2534.32	First Tangential, 2612.0	47	23	11913.05	
3	1	2534.32		48	24	11917.61	
4	2	2584.73		49	24	11917.61	
5	2	2584.73		50	25	11917.83	
6	3	2596.42		51	25	11917.83	
7	3	2596.42		52	26	11917.93	
8	4	2601.00		53	26	11917.93	
9	4	2601.00		54	27	11918.22	
10	5	2604.00		55	27	11918.22	
11	5	2604.00		56	28	11918.45	
12	6	2606.20		57	28	11918.45	
13	6	2606.20		58	29	11918.58	
14	7	2606.96		59	29	11918.58	
15	7	2606.96		60	30	11917.74	
16	8	10058.24	Tang. Fixed Support-1, 10150.0	61	30	12009.45	Tang. Fixed Support-4, 12030.0
17	8	10058.24		62	31	12004.48	
18	9	10060.23		63	31	12004.48	
19	9	10060.23		64	32	12008.13	
20	10	10063.98		65	32	12008.13	
21	10	10063.98		66	33	12008.21	
22	11	10068.76		67	33	12008.21	
23	11	10068.76		68	34	12008.35	
24	12	10071.97		69	34	12008.35	
25	12	10071.97		70	35	12008.54	
26	13	10046.87		71	35	12008.54	
27	13	10046.87		72	36	12008.70	
28	14	10130.79		73	36	12008.70	
29	14	10130.79		74	37	12009.42	
30	15	10121.95		75	37	12009.42	
31	15	11631.97	Tang. Fixed Support-2, 11678.0	76	38	12031.96	Tang. Fixed Support-5, 12049.0
32	16	11632.38		77	38	12031.96	
33	16	11632.38		78	39	12032.06	
34	17	11633.01		79	39	12032.06	
35	17	11633.01		80	40	12032.07	
36	18	11634.16		81	40	12032.07	
37	18	11634.16		82	41	12032.09	
38	19	11635.02		83	41	12032.09	
39	19	11635.02		84	42	12032.10	
40	20	11635.66		85	42	12032.10	
41	20	11635.66		86	43	12032.11	
42	21	11636.07		87	43	12032.11	
43	21	11636.07		88	44	12032.12	
44	22	11636.27		89	44	12032.12	
45	22	11636.27		90	45	12032.06	

The following important points for the packeted bladed disk can be made based on the results presented:

- The disk is considered infinitely stiff in the tangential direction. Therefore, the natural frequencies in the tangential mode of vibration of the bladed disk are expected to be very close to that of the cantilevered packet.
- The expected number of modes is 90 for the packeted bladed disk for this tangential vibration because there are 90 blades.
- There are 15 modes of the bladed disk that exhibit the same mode for each packet. This equals the number of packets on the disk.
- There will be six groups of modes in which the packet will exhibit the same displacement pattern because there are six blades in a packet. There are six basic modes for a packet containing six blades. This will make a total of 90 (15 × 6 = 90) modes.
- The largest magnitude of the packeted bladed disk frequencies of a group must be less than the frequency of the cantilevered packet blades.
- Certain mode shapes normally having two equal frequencies for a symmetrical structure will split into two frequencies. This phenomenon is called "splitting of modes." This is due to mistuning arising from breaking shrouds in 15 packets. For example in this case the 15 ND mode and 30 ND mode have split into two frequencies.

Completely Shrouded Design

Many turbine stages have blade tips joined by a single shroud band with the two ends of the shroud joined together. This construction is called a "completely shrouded" (360 degree shroud) design. The vibration characteristic of this design is similar to that of a single blade design. The difference is that there is a coupling between blades through the shroud band. The shroud provides stiffness to the system, raising the frequency. The frequencies of a completely shrouded design are higher than those exhibited by a freestanding design. The highest frequency is expected to be less than that of a single cantilevered packet containing all blades. Figure 10 graphically demonstrates this behavior.

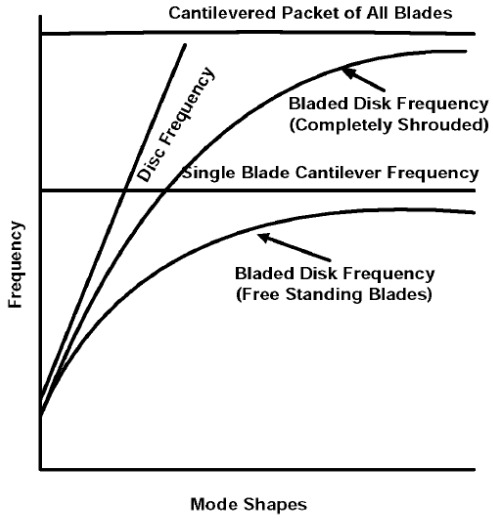

Figure 10. Behavior of Completely Shrouded and Free-Standing Bladed Disks.

Summary of All Bladed Disk Designs

The vibration of bladed disks can be summarized based on the following:

- A free standing blade design yields the lower limit of frequencies.
- A completely shrouded design yields the upper limit of frequencies.
- A packeted bladed disk design falls between the shrouded and the free standing design.
- A cantilevered single blade frequency is the upper limit for the free standing blade frequency.
- A cantilevered packet frequency is the upper limit for bladed disk frequency.

EVALUATION CONCEPTS FOR BLADE RESONANT VIBRATION

Campbell Diagram

The strategy for blade design is to avoid the coincidence of the harmonics of running speed and nozzle passing frequencies with the natural frequency of the blade (Figure 11). The concept of resonance where the mode shape and the shape of the force also play a defining role is explained later in this section. The following example of the Campbell diagram is instructive to demonstrate that if the shape of the force and mode shape are identical and the natural frequency is also equal to the frequency of the exciting force, the magnitude of the response will be large. However, the blade will also respond to forces even if the frequencies are not equal, but clearly, the response will be very small. Resonant response is inversely proportional to damping.

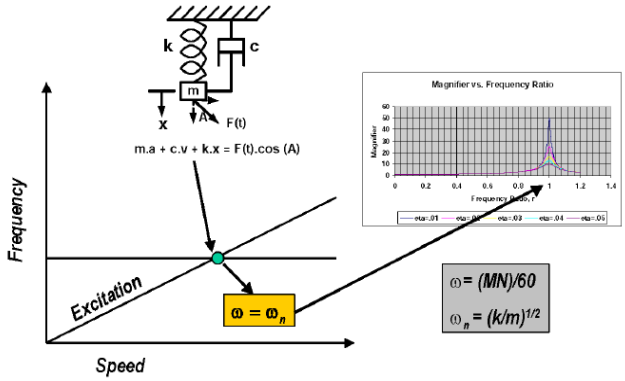

Figure 11. An Explanation of a Campbell Diagram.

The basis of the validity of a Campbell diagram can be explained by examining the equation of the magnifier that was presented earlier. The key point is that when the frequency ratio is equal to unity, the response of the system is the largest. Natural frequencies of the system are calculated by suitable analysis or are measured by testing.

The frequency of the exciting force is a function of the speed of rotation and the number of interruptions in the flow field. It is implied in the figure that the shape of the force is identical to the natural mode shape. This assumption might not be realized in every instance of coincidence of frequencies as might be inferred from the Campbell diagram. Two conditions are essential for a true resonance to occur:

- The frequency of the exciting force equals the natural frequency of vibration, and
- The profile (shape) of the applied force has the same shape as the mode shape associated with that natural frequency.

Mathematical expressions also provided support the case that each of the above conditions is necessary for resonance to occur but not sufficient in itself. For resonance to occur, both conditions must be satisfied at the same time. The time varying periodic forces experienced by rotating blades can be resolved in harmonics. Resolution of harmonics is accomplished by performing Fourier decomposition of the periodic force shape. The frequencies of the harmonics are an integer multiple of the speed of rotation. In

general, the force experienced by the blades of a turbine disk during a complete revolution is the consequence of any circumferential distortion in the flow field, etc.

The frequency of the excitation due to nozzle vanes or due to struts or any obstruction in the flow field is given by:

$$k.\omega = (K.N)/60 \quad (4)$$

where:

k.ω = Frequency of the exciting force, Hz
K = Number of distortions in the flow per 360 degrees, e.g., number of nozzles, or number of struts in the flow field, etc.
N = Turbine speed, rpm

K represents the shape of the excitation at the k nodal diameter.

The K_{th} harmonic of the force felt by the blades can be written as:

$$P_k(\theta, t) = P_k \operatorname{Sin} k(\omega t + \theta) \quad (5)$$

Where the frequency of the force is kω and θ is the angle on the disk from a reference point. The mode shape with m nodal diameters and with the natural frequency (ω_m) can be expressed as:

$$X_m(\theta, t) = -A_m \operatorname{Cos}(\omega_m t + m\theta) \quad (6)$$

The condition of resonance can occur when the alternating force does positive work on the blade. Work done is a function of displacement and is expressed as dW = P(x).dx. The work done by the k_{th} harmonic of the force acting on a mode shape having m nodal diameters in one complete period (T) can be expressed as follows:

$$W = \int_0^{2\pi}\int_0^{T} P_k(\theta,t)\ \frac{d}{dt} X_m(\theta,t)\ \frac{N}{2\pi}\, dt\, d\theta = \int_0^{2\pi}\int_0^{T} P_k \operatorname{Sin} k(\omega t + \theta)\omega_m A_m \operatorname{Sin}(\omega_m t + m\theta)\ \frac{N}{2\pi}\, dt\, d\theta \quad (7)$$

$$= \begin{cases} N\pi P_k A_m & (\text{for } m = k \text{ and } \omega_m = k\omega) \\ 0 & (\text{For either } m \neq k \text{ or } \omega_m \neq k\omega) \end{cases} \quad (8)$$

The first expression of Equation (8) is the positive work ($N\pi P_k A_m$) done by the force. This is true only if the nodal diameter (m) of the mode shape is the same as the shape of the k_{th} harmonic of the force and the natural frequency (ω_m) of vibration is equal to the frequency (kω) of the force.

Zero work results when either the nodal diameter (m) of the mode shape is not the same as the shape of the k_{th} harmonic of the force or the natural frequency (ω_m) of vibration is not equal to the frequency (kω) of the force. The above argument is the basis of the interference diagram and it further explains the need to examine the frequency of vibration and the mode shape and the shape of the force when considering resonance.

A simple way of understanding the implications of Equation (8) is by examining the behavior of a multidegrees of freedom system containing spring and mass.

Examine the three springs and masses system depicted in Figure 12. Each mass represents a degree of freedom therefore this is a three degrees of freedom system. The degree of freedom is displacement (motion) in the vertical direction. There will be three natural modes and three associated natural frequencies (ω_{n1}, ω_{N2}, ω_{N3}). The first mode depicts each mass moving in the same direction at any instance during vibration cycle. Figure 12 shows these masses move downward. The second mode depicts displacement of first two masses as downward but the third mass moves in the upward direction. The third mode shows first mass as moving downward, second mass moving upward, while the third mass moves downwards. In the first mode there is no phase difference among the motion of masses. During vibration in the second mode there is one phase change while in the third mode phases change two times as one should expect.

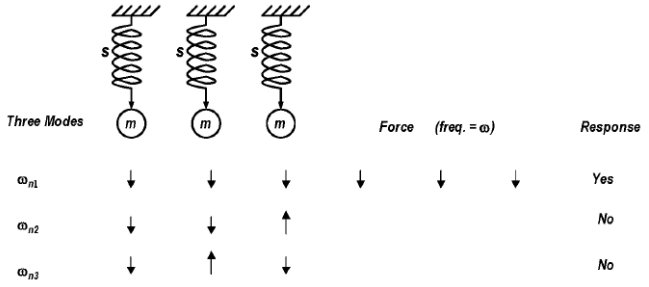

Figure 12. Three Degrees of Freedom System, Shapes and Frequencies (ω = ω_{n1}) Match.

Assume a force is being applied to three masses as shown. Force at each mass is applied in the direction of motion with a frequency of ω. There is expected to be a resonant response of the system when ω = ω_{n1}. This example meets both conditions as required by the first part of Equation (8), i.e., shape of the force matches with the mode shape and the excitation frequency (ω) equals the natural frequency (ω_{n1}).

The same condition is shown in Figure 13 but the shape of the force does not match the mode shape. There is no response of the system even though the excitation frequency equals the natural frequency. However, as expected, the second mode responds under the action of this force. If the excitation frequency is not equal to the natural frequency, then there is no response (Figure 14). When ω = ω_{n2}, there will be response as depicted in Figure 15.

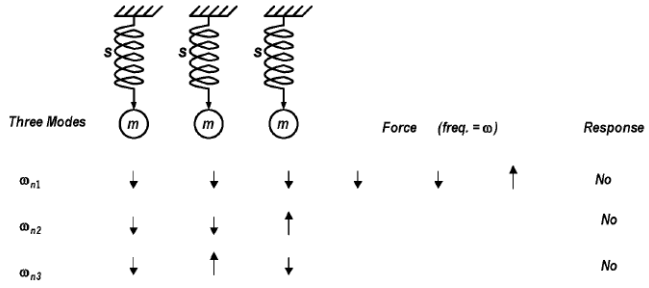

Figure 13. Three Degrees of Freedom System, Shapes Do Not Match and Frequencies (ω = ω_{n2}) Are Equal.

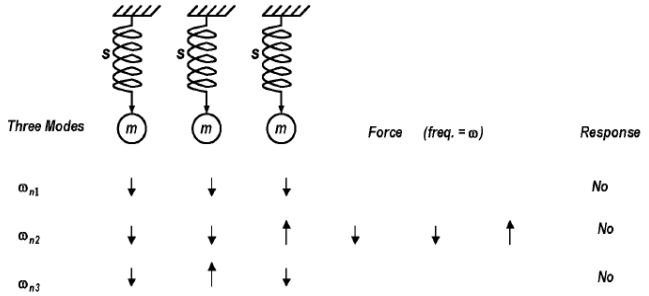

Figure 14. Three Degrees of Freedom System, Shapes Match and Frequencies Are Not Equal.

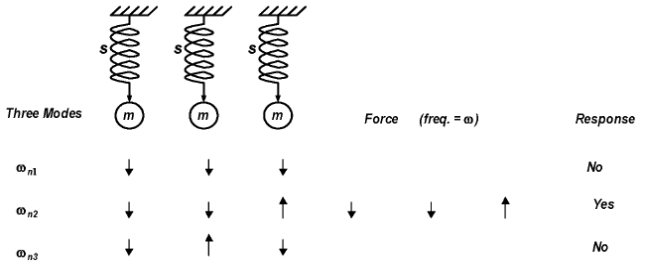

Figure 15. Three Degrees of Freedom System, Shapes and Frequencies ($\omega = \omega_{n2}$) Match.

Examples of Figures 12 and 15 meet both conditions as expressed in the first part of Equation (8). Examples of Figures 13 and 14 show the cases of the second part of Equation (8), thereby no response is expected.

Interference Diagram—SAFE (Singh's Advanced Frequency Evaluation) Diagram

To describe the dynamic behavior, two pieces of information are essential, mode shape and natural frequency. Singh and Vargo (1989) described a method of using this information to create an interference diagram for a packeted bladed disk. The interference diagram combines bladed disk natural frequencies, bladed disk mode shapes, excitation frequencies, and operating speeds on one graph. It is an excellent guide to determine the potential of exciting a particular mode of vibration. In any vibration cycle, certain parts of a mechanical structure remain stationary. For a circular symmetric system, these points fall on radii (always an even number) or circles. A pair of radii (opposite each other) is considered as a diameter. Mode shapes can be characterized by specifying the number of nodal diameters (ND) and nodal circles (NC). The x-axis of the diagram represents nodal diameters. The frequency is plotted on the y-axis of the interference diagram. A good design would yield an interference diagram that indicates no coincidence of possible excitation force with a natural mode of the bladed disk. An understanding of the details of the interference diagram for a particular mode shape is essential for determining the likelihood of exciting that particular mode to a degree where it will adversely affect reliability.

The results of the modal analysis are used to draw an interference diagram. The analytical results generate natural frequencies and associated mode shapes. Shape of deflections around the disk and cover are calculated by using a Fourier decomposition method to identify the mode shapes in terms of nodal diameter.

In the case of an axisymmetric system, modes occur in pairs except for the first mode called 0ND, which is always single. In addition, the total number of modes must be equal to the number of blades on the disk. For constructing any interference diagram (SAFE diagram) it is important that:

- The maximum number of nodal diameters is equal to half of the number of blades when the number of blades is even. For the case of a stage having 90 blades, the largest nodal diameter mode will be 45 (90/2).
- The maximum number of nodal diameters is half of one less than the number of blades when the number of blades is odd. If the stage has 91 blades, the largest nodal diameter mode will be 45 ((91-1)/2).
- The last nodal diameter mode will be single in the case of an even number of blades.
- The last nodal diameter mode will be double in the case of an odd number of blades.

The results of the Fourier analysis on displacement can be divided into axial and tangential directions, depending on the dominant deflection of each mode. The description of mode shapes by nodal diameters is a key element in the construction of the interference diagram. It is essential for understanding how a structure can be excited when introducing a periodic stimulus to the blades. The mode shapes in the first family will consist of each blade displaying the first bending mode of a single blade.

For true resonance, coincidence of frequencies is required and the shape of the exciting force must match the mode shape at the same time. As usually drawn, examination of a Campbell diagram can only infer coincidence of frequency. Thus, the Campbell diagram is overly conservative and can predict the intersection of excitations that is not physically possible. Avoidance of such intersections can restrict the design without any real value.

The interference diagram (e.g., SAFE diagram) includes information about frequencies as well as the shapes. Hence, it depicts a much more accurate condition for a true resonance interference. To draw an interference type diagram (SAFE diagram), the following information is required:

- Natural frequencies of bladed disk (it should be recognized that these frequencies might depend on speed of rotation and temperature of the blade. The effect of speed is not easily displayed on a SAFE diagram).
- Mode shape of the bladed disk defined as nodal diameter.
- Sources of excitation must be known, e.g., number of nozzles, number of struts, etc.

A SAFE diagram can be constructed as follows:

- The mode shape as nodal diameter is plotted on the horizontal axis. The natural frequencies are plotted on the vertical axis.
- The equation of the force (mentioned earlier $\omega = (K.N)/60$) is used to draw the frequency of the excitation line for a given speed as a function of the nodal diameter. This is a radial straight line starting from the origin.
- The frequency of the exciting force is drawn as a vertical line between the operating speed range at the ND denoting the shape of the force, e.g., for 36 nozzles the 1×NPF is drawn at 36 ND.

The data of Table 2 was used to construct the SAFE diagram of Figure 16.

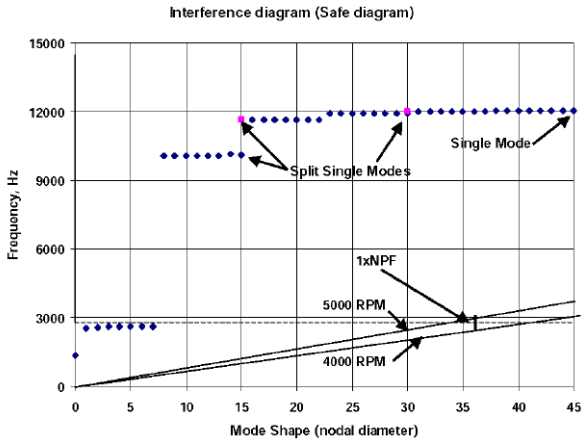

Figure 16. Interference Diagram (SAFE Diagram).

There are two basic pieces of information displayed on the interference (SAFE) diagram. Points on the diagram represent the mode and frequency of the bladed disk system. The exciting force is displayed as a vertical line between the operating speed range at the nodal diameter representing the shape of the force. For "resonance" to occur, the frequency and shape of the exciting force and the bladed disk must be identical.

Simply stated, there should not be any concern if the vertical line (representing force) does not pass through a point (representing bladed disk vibration) as shown in Figure 16. The same data when plotted on a Campbell diagram discussed earlier (Figure 11) raise concern. The shape of the force and the mode shape of vibration were not taken into account in the Campbell diagram.

Interference Diagram When Harmonics of Excitation Is Larger than Half of the Number of Blades

SAFE diagram plots modes up to half of the number of blades. There are situations where the harmonic of excitation may be larger than the maximum mode shape plotted on the diagram. For example 2×NPF excitation relates to a harmonic of 72 ND. Maximum mode shape displayed on the diagram is 45 ND. The question to be answered is whether this excitation may excite any mode displayed on the diagram.

Examine the two sine plots of Figure 17. The subtended angle between blades is 4 degrees for a stage that has 90 blades. It is clear from the plot that these two waves intersect at precisely 4 degrees. The implication is as follows: if each blade is instrumented to measure and thereby to determine the shape of the fluctuating force in each revolution, then both waves are equally probable. This means that a 18-nodal diameter mode of the bladed disk may be excited by a force that has a 72-nodal diameter shape, provided that the frequencies are the same. There are many combinations for which this assertion is true but the combination is unique for each individual bladed disk. The combination, however, depends on the number of blades in the stage. Another such combination for this disk is a 10 nodal diameter mode that may be excited by a force of an 80-nodal diameter shape if the frequencies are the same (Figure 18).

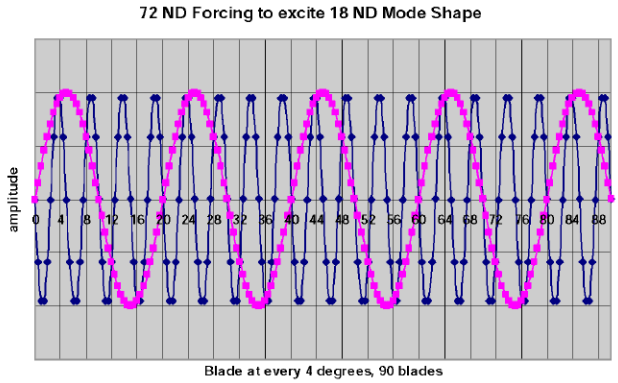

Figure 17. Sin(18θ) and Sin(72θ).

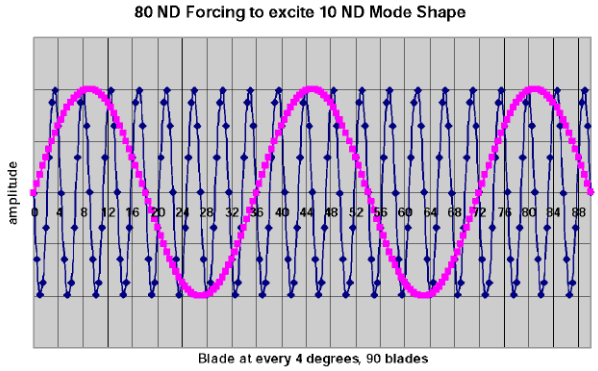

Figure 18. Sin(10θ) and Sin(80θ).

A mode shape and the shape of the excitation should be the same for resonance to occur. Consider a case where the nodal diameter (the shape of the excitation) is larger than the maximum nodal diameter of the mode shape just discussed. For example, assume that the number of nozzles used for the design is 36. The shape of the 2×NPF excitation is 72. The question is "will the force resulting from 2×NPF excite any bladed disk mode that is less than 45 nodal diameters?" This situation is graphically shown in Figure 19. Even though 45 ND is the maximum shape representation required for bladed disk vibration of 90 blades, the shape of the exciting force may be larger than 45 ND. This is the case for this example. The 2×NPF excitation shape is 72 ND. This phenomenon (aliasing) is taken care of on the SAFE diagram by folding the radial speed lines as shown in Figure 20.

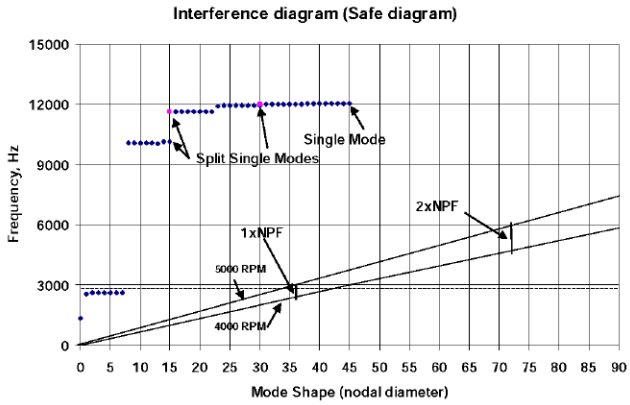

Figure 19. Excitation Shape Larger than Blade Mode Shape.

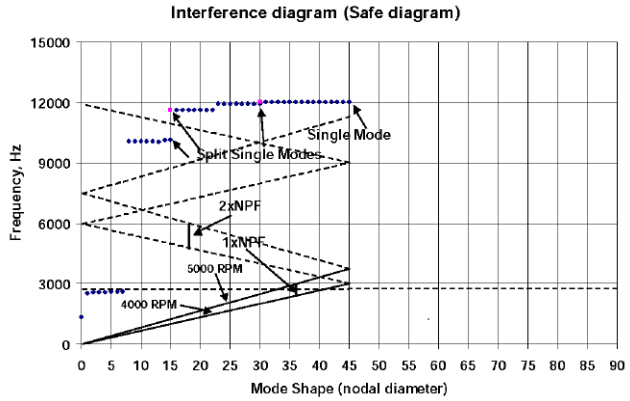

Figure 20. Reflected Speed Lines.

Singh (2006) provided the following relationships for possible combinations:

$$K = \text{abs}(n.L + M) \text{ and} \tag{9}$$

$$K = \text{abs}(n.L - M) \tag{10}$$

where:
K is the shape of the force (nodal diameter)
n is 0, 1, 2, 3, …, L
L is the total number of blades
M is the nodal diameter of mode shapes

MISTUNING OF A BLADED DISK SYSTEM

Mistuning can be considered as any irregularity in the bladed disk system that makes the response of the system asymmetric. These irregularities can be caused by structural and/or aerodynamic means. This causes force around the periphery of the disk to be of a nonsinusoidal form.

Structural mistuning results in a phenomenon called "splitting of frequency." For a tuned system, frequencies occur in duplicate, i.e., there are two frequencies for a given mode shape. These shapes are graphically the same but differ from each other by a phase angle.

Splitting separates these frequencies for each mode. The amount of separation of frequencies depends on the amount of mistuning. For example a three nodal diameter pattern of a disk might occur at two frequencies. In general, these frequencies crowd the Campbell diagram. The interference diagram yields a better depiction of this phenomenon.

The analysis of a mistuned bladed disk system becomes complex. Due to manufacturing variations, blades on the same disk will be different from each other even when they are within manufacturing tolerances. Their contact condition in the disk slot may also be different. Therefore, assembly of these blades on a disk will be random unless each blade is individually measured and its location on the disk noted. Even known locations pose difficulty in analysis. It should be recognized that each bladed disk produced in such a manner from the same lot of blades will be different and, therefore, their vibration characteristics will also be different. The complexity of the analysis is compounded by the presence of a large number of blades on the disk.

Ewins (1969) reported that for given excitation and damping conditions, the response in one mode (or pair of modes) depends on the "split" of the two natural frequencies. The presence of slight mistuning—small blade imperfections—can cause resonant stress levels of up to 20 percent above the optimum. This kind of increase depends on the specific arrangement of the blades around the disk. Singh and Ewins (1988) and Singh (1992) presented probabilistic analysis results by considering a random arrangement of blades on the disk. A Monte Carlo simulation was used to arrive at the results.

The analysis reported earlier for the packeted bladed disk may be considered as deliberate mistuning. This was achieved by breaking a continuous shroud band into packets at predetermined locations. This method permits known modes to be split and has been used successfully in packeted bladed disk design.

For a mistuned bladed disk system, the vibration energy is unevenly distributed among all blades of the disk. The mode shapes may be far from a regular sinusoidal shape. The examination of modes in such a situation is done using Fourier decomposition of the displacement pattern in harmonic content. The mode is traditionally named in accordance with the largest content of the harmonics of the Fourier decomposition.

USE OF CFD IN AIRFOIL DESIGN

It has been nearly 200 years since Navier and Stokes introduced the equations that bear their names. It has taken this length of time to develop the computing capability needed to solve those equations in a timely fashion. However, the use of CFD in turbomachinery airfoil design traces its roots to the late 1970s.

Prior to that time, airfoil sections were designed using simplified techniques that could be executed by hand using slide rules and early mainframe computers. Once designed, these airfoil sections were tested in cascade tunnels to verify their performance. To this day, some turbomachinery analytical codes use cascade data subroutines to infer the performance of "standard series" airfoils.

Early numerical methods were inviscid Euler codes. The Euler equations are essentially equivalent to the Navier-Stokes equations, but without viscosity and heat conduction. These codes were used to design airfoils in 2-D slices, a method called blade element analysis that is still used today. Boundary layer solutions were superimposed on the inviscid surface Mach number distribution to calculate losses. 3-D Euler codes, which modeled an entire blade from hub to tip, were developed soon after. However, the difficulty of manipulating airfoil geometry in three-dimensional space (both in terms of airfoil geometry generation codes and designer visualization) ensured that these codes were mainly used to analyze blades designed with 2-D methods.

Potential flow solutions, which are also inviscid, allowed better solutions for subsonic cases where shocks were not an issue. Just as with the Euler codes, a boundary layer solution was superimposed over the inviscid surface Mach number distribution generated for a blade element.

In the late 1980s, true Navier-Stokes solutions were being developed. It is these solutions that are typically referred to as CFD. CFD codes can be used as the solver in a 2-D blade element design, or in a full 3-D analysis mode. Early CFD codes could only handle a single blade or vane row. As computing capability increased, stages could be analyzed, then entire flow paths, and currently, entire machines can be modeled, including leakage flows. However, the larger the model, the greater the node count, and the longer the model takes to converge on a solution (a node is a point in space where X, Y, and Z grid lines intersect). There are also potential grid issues with complex models in that the model can have very small grid elements and very large grid elements in the same model. Generally, codes tend to run better when all the grid elements are of similar size. Of course, this is never the case, but the greater the size disparity, the more difficulty the code will have in arriving at a solution.

CFD permits the designer to see flow features that could not be studied using previous methods. The drawback to CFD is that it is very grid dependent. The CFD solution obtained from a model is at least as dependent on the solution grid as it is on the boundary conditions. For this reason, prior to running a new model it is extremely important to calibrate a CFD model with a known solution of a similar design, preferably one with test data available. This ensures that the solution is being driven by the physics of the problem, and not in the numerical solutions. If the solution is independent of the grid, by doubling the node count and rerunning the model, the solution will not vary with the additional nodes.

Since the 1990s, various attempts have been made to incorporate adaptive grids into CFD codes. Adaptive grids allow the code to automatically increase the grid density where the solution experiences large gradients. A successful adaptive grid methodology would remove the grid dependency issues from CFD solutions.

In addition to grid density issues, the CFD user must be careful to choose appropriate turbulence modeling for the design in question. Again, it is important to verify the selection of a turbulence model by calibrating the solution against a baseline model (preferably one with test data available).

Finally, one of the most powerful uses of CFD is to combine CFD modeling with a test program that includes flow visualization. The combination of test flow visualization coupled with CFD modeling can illustrate flow features that would otherwise go undiscovered.

The increased capacity and availability of computing power have been responsible for a considerable portion of the growth of CFD applications and will continue to permit advances in the successful application of this technology.

DAMPING CONCEPT

More adequate damping can minimize dynamic stresses of the disk system. The system damping is the sum of mechanical and aerodynamic damping. Materials under cyclic loading absorb energy, some of which may be stored as potential energy but most of which is dissipated as heat. The amount of this energy may be small and it may be very difficult to measure.

Energy dissipation in materials, termed damping, is caused by many physical mechanisms that depend on the material, temperature, applied stress and the frequency of the cyclic loading. Damping behavior is of practical importance as the amount of damping affects the response under vibratory loading. Higher damping reduces the stresses in forced vibration near resonance and is also responsible for the decay of free vibration.

The rheological model exhibits the behavior of low stress damping (Figure 21).

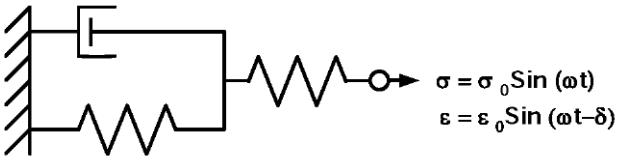

Figure 21. Rheological Model for Damping.

$$\sigma = \sigma_a \, \mathrm{Sin}\, \omega t \tag{11}$$

where:
σ_a is the stress amplitude
ω is the frequency

The strain (displacement) response is sinusoidal with a phase shift (angle, δ) relative to the stress.

$$\varepsilon = \varepsilon_a \, \mathrm{Sin}\, (\omega t - \delta) \tag{12}$$

The stress-strain response forms an elliptical hysteresis loop. The area of this loop is the dissipated energy ()u) in each cycle per unit volume.

$$\Delta u = \pi \, \sigma_a \varepsilon_a \, \mathrm{Sin}\, \delta \tag{13}$$

Pure sinusoidal force frequently used in the analysis of a vibrating system is uncommon in practice. Many harmonics of the force are present that distort the form of the force. The characteristics of the forcing function may significantly affect the damping properties of materials during periodic vibrations. Some of the factors that may affect the damping properties are listed below.

- Form of the force
- Frequency
- Amplitude of the force
- Ratio of alternating to mean stress
- State of stress—uniaxial or multiaxial
- Prior stress history
- Temperature
- Radiation
- Environment

The absorbed damping energy is generally dissipated as heat. A small portion of the damping energy may be absorbed by structural change that raises the energy level of the system. The discussion here is limited to “mechanical damping,” i.e., the energy dissipation within a material or members under cyclic loading. This also includes energy loss at an interface that may occur during relative motion.

- For a complete system, $D_s = F\, dx$ (integrated over complete cycle)
- For material, $D = \sigma\, d\varepsilon$ (integrated over complete cycle)

D_s is the total energy absorbed per cycle of loading by the entire structure (in-lb/cycle)
D is the unit energy absorbed by a macroscopically uniform material per unit volume per cycle of loading (in-lb/in^3 cycle)

Another important relationship between the energy dissipation and stress amplitude when all other conditions are equal is stated below:

$$D = J \sigma^n \tag{14}$$

J and n are material constants. J is the damping constant and n is the damping exponent.

It has been observed that low stress amplitude leads to two conditions worth noting:

- Damping exponent n = 2, and
- The hysteretic loop is elliptical in form. This is termed “linear damping” and these conditions characterize linear viscosity (DASHPOT).

Viscous Damping

Previous treatment of a spring mass model system used the viscous damping model to solve the vibration behavior. The basic differential equation was:

$$m\,a + c\,v + k\,x = 0 \quad \text{for free vibration.} \tag{15}$$

The solution for frequency is given by:

$$\begin{aligned} \omega_1 &= -c/(2m) + ((c/2m)^2 - k/m)^{1/2} \\ \omega_2 &= -c/(2m) - ((c/2m)^2 - k/m)^{1/2} \end{aligned} \tag{16}$$

Critical Damping

The value of c that reduces the radical to zero in the above equation is called the critical damping, c_c.

$$c_c/2m = (k/m)^{1/2} = \omega_n \tag{17}$$

$$c_c = 2m\,\omega_n \tag{18}$$

The damping ratio defined earlier is:

$$\zeta = c/c_c \tag{19}$$

Proportional Damping

Sometimes for convenience of analysis, a particular type of damping concept is used called “proportional damping.” The mathematics for analyzing the example with viscous damping earlier was rather cumbersome. In this case the damping ratio, c, is assumed to be proportional to the stiffness and mass.

$$c = \beta\, k + \gamma\, m \tag{20}$$

where β and γ are damping ratios.

Many ways of defining damping have been used for mathematical formulations of vibration problems. Some are based on test data and some on concepts developed based on physical principles. The relationship between them is summarized below for convenience. If $\Delta\omega$ is the difference in frequency at the half power point, δ = log decrement, ζ = ratio of damping coefficient to critical damping, Q = amplitude factor, then:

$$\eta = \Delta\omega/\omega = \delta/\pi = 2\zeta = 1/Q \tag{21}$$

Frictional Damping

Damping to reduce the vibration amplitude is induced by rubbing actions at the mating surfaces in many mechanical systems. Sometimes this type of damping due to mating surfaces is introduced deliberately so that relative motion will provide a resisting friction force and also generate heat to dissipate energy. Heat is dissipated in friction and the friction force opposes the relative motion at the interface. This is a characteristic of slip and stick motion. There has been much effort in the last two decades to develop analytical procedures to solve active damping near the blade and disk interface.

The physical mechanism of the phenomena that occur between contacting surfaces is not well understood. During dynamic motion the contacting surfaces go through micro slip, gross slip, stick, and slip motion. Some of the parameters known to influence this behavior include the normal force trying to hold surfaces together, characteristics of surfaces, material properties, surface roughness, surface treatment, frequency of vibration, and coefficient of dynamic friction. This makes the phenomenon completely nonlinear. Attempts have been made to analyze the phenomenon by approximating it as a linear process. Surfaces resulting from manufacturing are rough and contain asperities. Normal load crushes these asperities and the contact is taken as the average of the crushed area on which the load is assumed to be acting. Contact will increase with increasing load thereby further deforming the asperities. The resistance to slip motion is proportional to the number of these asperities. There is energy that is also dissipated by rupture of the frictional bond. Heat is also generated at the cost of energy being input. Utilization of the simple law of friction with tangential force, $F = \mu N$, even when applied to a single degree of freedom system, provides complications. Some advanced methods (Sanliturk and Ewins, 1996; Menq et al.; Griffin and Menq, 1991) have attempted to accurately represent the behavior in a vibrating system and have shown promise.

Many designs have shroud constructions called Z lock. Figure 22 shows such an arrangement. The geometry of a shroud is such that it mates with the adjacent shroud through an interface. This contacting surface is assembled with a preload providing a normal acting force.

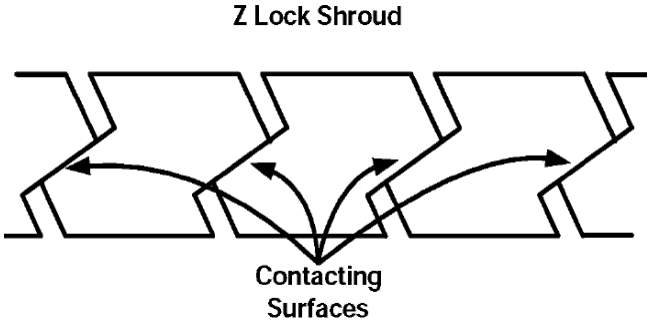

Figure 22. Z Lock with Contacting Surfaces.

The precise conditions and the consequent effects continue to be an unsolved problem. At operating speeds blades untwist and the interface condition changes from the assembly condition. The dynamic motion of one shroud relative to its neighbor provides tangential resistance and energy dissipation. Many of the analytical approaches mentioned earlier may be used to theoretically evaluate its effectiveness. However, test results should provide a better estimate of the damping magnitude by measurement of the response at any speed or mode of vibration.

It is clear that the physical phenomenon of active damping is not well understood even though many researchers are actively working to understand it. However, for practical applications, the following is a brief description.

Figure 23 shows plots of response in a situation of interface friction. The first curve shows the condition for which there is no contact. When the friction force is large enough, then the interface contact might get stuck, i.e., it behaves like a solid interface. In this situation, the frequency is larger than that of the no contact case. Depending on the contact situation, the response curve is assumed to fall in between these two cases with decreased amplitude depending on the effective damping.

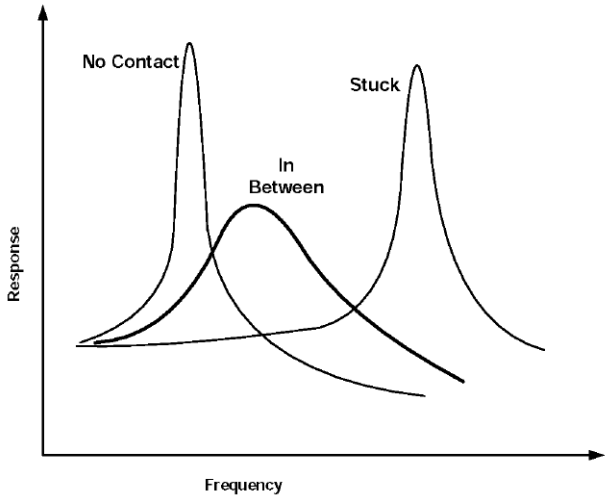

Figure 23. Response Curves for Different Contact Conditions.

Consider a continuous shroud case where the displacement of the shroud during vibration should be a continuous pattern as shown in Figure 24. Construction with individual shrouds might displace as shown in Figure 25. During each cycle of vibration, the shroud of one blade will rub against the adjacent shrouds. The friction force will depend on the contact condition, e.g., the normal force. The force system acting on the interface is shown in Figure 26. The tangential force provides the resistance to motion.

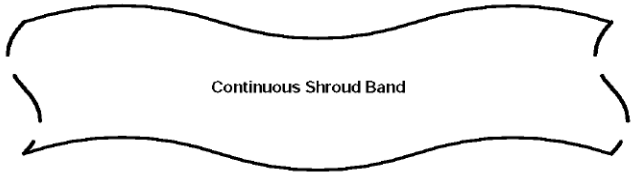

Figure 24. Displacement of a Continuous Shroud Band.

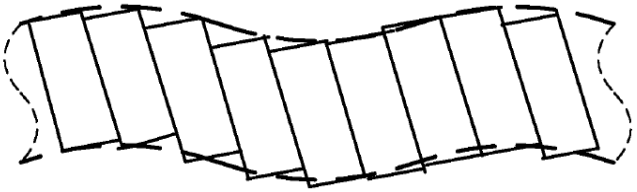

Figure 25. Displacement of Individual Mating Shrouds.

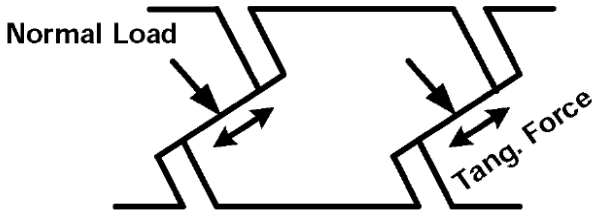

Figure 26. Loads on Mating Surfaces.

One can visualize three distinct conditions at the contacting interface—micro slip, macro slip, and completely stuck. The tendency might be to design a large interference in an effort to introduce a large friction force. If not done wisely however, this might not work if the contact surface gets stuck. The only benefit in such a situation might be to increase the natural frequency. On the other hand, there might be a chance of fretting fatigue damage due to relative motion of the contacting surfaces. In this case, design is a balancing act.

ASSESSMENT OF THE USEFUL LIFE OF A BLADE IN THE PRESENCE OF HIGH CYCLE FATIGUE

The Industrial Revolution of the 1800s saw the advent of rotating and reciprocating machinery. The failure of metals due to repeated loads became a recognized problem. Ductile metals failed in a brittle manner. Failures occurred at loads that were considered to be "safe." These failures were a surprise. Subsequent investigations identified the concept of fatigue failures, where the failure is due to a combination of load and load cycles.

The vast majority of component failures in ground, air, and sea vehicles are now attributed to fatigue failure. Most blade failures are the result of the application of a cyclic load. Thus, considerable effort and resources are expended in dealing with and avoiding/alleviating fatigue problems. This section describes some of the key aspects that need to be considered in blade design.

Consider the behavior of a material under cyclic load where the amplitude of the stress is above the elastic limit or yield strength of the material. After unloading, the material does not return to its original position and there is a permanent deformation. Test data show a hysteresis loop when a material is subjected to repeated cycle loads. The area of the loop is proportional to the work that has not been recovered. In essence, it represents the energy that has been stored in the material. Figure 27 shows such a hysteresis loop. The plot of the strain range versus cycles to failure is also shown in the Figure 27. It is similar to the well-known S-N curve for the material.

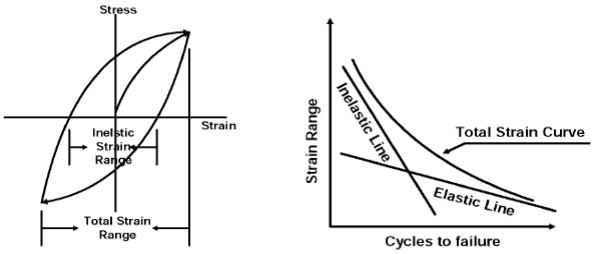

Figure 27. Hysteresis Loop During Cyclic Loading.

The total strain range consists of the elastic strain, i.e., that recovered after unloading and an inelastic strain, i.e., that not recovered after unloading.

- Total strain = Elastic strain + plastic strain

The test data of many steels plot as straight lines for both strains (elastic and inelastic) versus cycles to failure on a log-log scale. Equation (22) is such a relationship, known as the Manson-Coffin relationship when the mean stress is zero.

$$\Delta\varepsilon Total / 2.0 = A N_f^b + C N_f^d \quad (22)$$

Morrow modified the above equation to include the effect of mean stress as follows:

$$\Delta\varepsilon Total / 2.0 = ((\sigma_f' - \sigma_m) /E) N_f^b + C N_f^d \quad (23)$$

In the case of high cycle fatigue (hcf), the inelastic strain is considered to be negligible and therefore:

$$\Delta\varepsilon Total / 2.0 = ((\sigma_f' - \sigma_m) /E) N_f^b \quad (24)$$

This will be used as the basic relationship between the strain and cyclic life when the inelastic strain is negligible. For the purpose of the discussion that follows, this is considered to be the case for high cycle fatigue.

Techniques such as the Goodman diagram are used to estimate the safety of a mechanical structure under high cycle fatigue loading (Figure 28). The factor of safety (FS) indicates the margin from the acceptable nominal design. A value of FS greater than one is required to account for the uncertainty and variability in loads and material properties. FS based on stress does not provide any direct knowledge about the working life of the mechanical structure. A life estimate can be made in conjunction with the Goodman concept. This method provides an estimate of life employing the information used in constructing a Goodman diagram (Singh, 2001).

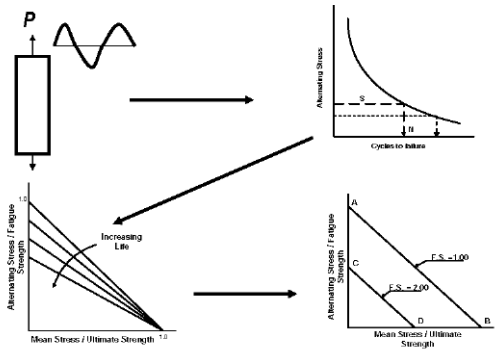

Figure 28. From Test Sample to Goodman Diagram.

Factor of Safety Concept for High Cycle Fatigue

The Goodman equation as given below accounts for the effect of mean stress on fatigue life:

$$\sigma_a / \sigma_e + \sigma_m / \sigma_{ult} = 1 \quad (25)$$

where:

σ_a = Alternating stress, psi
σ_e = Fatigue strength, psi
σ_m = Mean stress, psi
σ_{ult} = Ultimate strength, psi

Equation (25) represents a straight line as shown in Figure 29. Each radial line represents a life that corresponds to the magnitude of the fatigue strength, i.e., the magnitude of the alternating stress when the mean stress is zero.

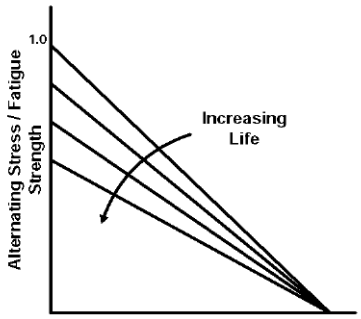

Figure 29. Goodman Diagram with Constant Life Lines.

A factor of safety based on stress or a margin is estimated by the following equation:

$$\sigma_a / \sigma_e + \sigma_m / \sigma_{ult} = 1 / FS \quad (26)$$

The plot of σ_a/σ_e versus σ_m/σ_{ult} (Equation (26)) is a straight line as shown in Figure 30 where line AB is the plot when FS equals 1.00 and line CD is for an FS of 2.00. Any combination of

alternating and mean stress that falls on line CD will have a factor of safety equal to 2.00. Figure 29 represents a life concept and Figure 30 represents the margin in the design when the permitted stresses are limited to a lower magnitude. The implication of Figure 30 regarding the life of the mechanical component can be observed in Figure 31. This shows a superimposition of Figures 29 and 30. The radial lines AF, BF, CF, DF, and EF represent constant life lines in increasing order. Line GH is a Goodman based factor of safety as defined by Equation (26). The intersecting points I, J, and K, although representing the same factor of safety, lie on lines denoting different life. Implication of this observation is that designs having the same factor of safety as defined by Equation (4) will yield different lives.

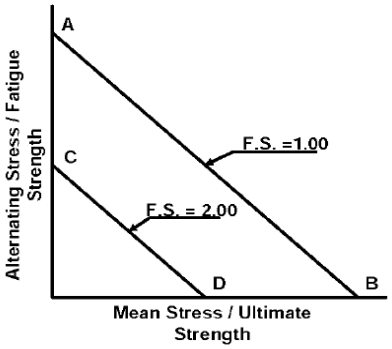

Figure 30. Goodman Diagram with Factor of Safety Line.

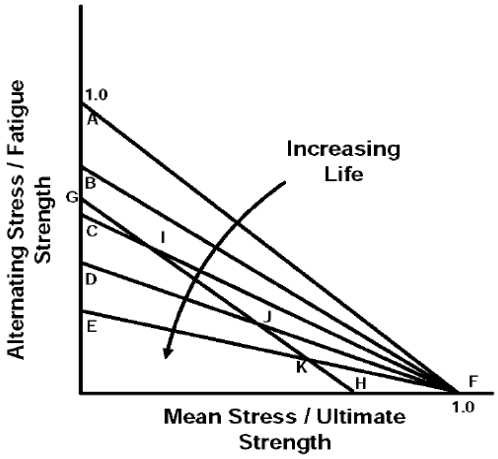

Figure 31. Superimposed Goodman Lines.

It is appropriate to use Morrow's equation to include the effect of mean stress on cycles to failure but neglecting the inelastic stress reduces it to:

$$\Delta\varepsilon_{Total} / 2.0 = ((\sigma_f' - \sigma_m)/E)\, N_f^b \quad (27)$$

where:

σ_f' = True fracture strength (true tensile stress to cause fracture)

$\Delta\varepsilon_{Total}$ = $(2\ \sigma_a)/E$, where σ_a is the alternating stress, half of the stress range

$$\sigma_a = (\sigma_f' - \sigma_m)\, N_f^b \quad (28)$$

In case of:

σ_m = 0

σ_a = σ_e

N_f^b = σ_e/σ_f'

After substituting and rearranging the above equation:

$$\sigma_a / \sigma_e + \sigma_m / \sigma_f' = 1 \quad (29)$$

For a constant life the relationship between σ_a and σ_m is a straight line as shown by Equation (29). The straight line is defined by the x-intercept of σ_f' and the y-intercept of σ_e. This equation has the same form as the Goodman equation. The difference is the use of s_f' in place of s_{ult} as in the Goodman equation. The Goodman line of Equation (25) and the straight line of Equation (29) are shown in Figure 32. Morrow's equation in essence estimates a longer life than that estimated using the Goodman radial line. Morrow's equation uses σ_f' (Point A) as the failure point compared to σ_{ult} used by Goodman.

$$\sigma_a / \sigma_e + \sigma_m / \sigma_{ult} = 1 \quad (30)$$

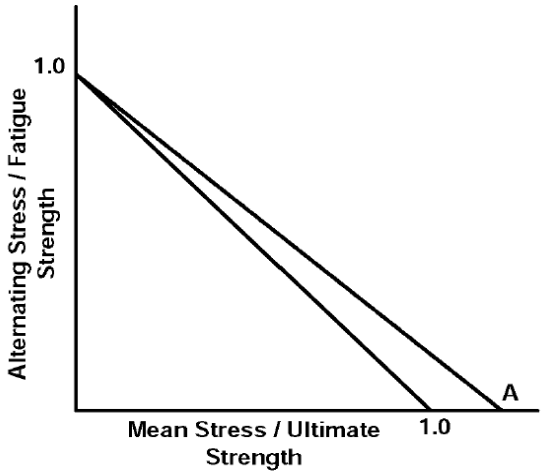

Figure 32. Comparison of Goodman and Morrow Equations.

By combining the Goodman equation and the life equation, an expression for the cycles to failure, N_f, for a specified FS is obtained and is given as:

$$N_f = ((1 / F.S - \sigma_m / \sigma_{ult})\,(\ \sigma_e / (\sigma_{ult} - \sigma_m)))^{(1./b)} \quad (31)$$

Similarly, N_f can also be expressed in terms of σ_a as given below:

$$N_f = ((\sigma_{ult} - \sigma_{ult}(1 / F.S - \sigma_a / \sigma_e)) / \sigma_a)^{(-1./b)} \quad (32)$$

LOW CYCLE FATIGUE

In the case of low cycle fatigue, life is limited by inelastic strains, i.e., where the hysteresis loop has an appreciable area for the given loading condition. In such a situation, the elastic strain may be neglected (Figure 33).

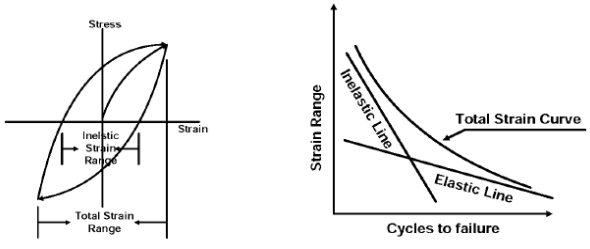

Figure 33. Cyclic Load and Strain Range Versus Life Curve.

- Total strain = Elastic strain + plastic strain

$$\Delta\varepsilon_{Total} / 2.0 = A N_f^b + C N_f^d = ((\sigma_f' - \sigma_m) /E) N_f^b + C N_f^d \quad (33)$$

The lcf damage is controlled by the plastic strain:

$$\Delta\varepsilon_{Total} / 2.0 = C N_f^d \quad (34)$$

PROBABILISTIC CONCEPT TO QUANTIFY THE RISK OF A PROPOSED DESIGN

"Probabilistic design is the codification of risk judgment; and *is not* the statistical analysis of the design problem." (James N. Siddall, McMaster University, Canada)

"There is a need for combining physics based theory of material behavior with probabilistic methods that account for uncertainty (variability) in data
a) To achieve a robust design, and
b) To estimate the risk in accepting the resulting design.

"No design has a 100% guarantee, i.e., absolutely no potential for failure. There is always a finite risk. Experience has shown this to be a fact." (Murari Singh, Safe Technical Solutions, Inc.)

Why probabilistic analysis?

- Tools are available to assess life.
- Consider uncertainties with appropriate physics based law(s).
- Probabilistic concept provides "estimate of risk."
- Finite life and an acceptable level of risk may be economic realities.

Drosjack, et al. (2005), described the need to move from today's concept of deterministic design to consider risk as a component in each design tomorrow. They pointed out the need to quantify risk. Risk is the likelihood of an event times the consequence of the event occurring. In deterministic design, various parameters are treated as single valued, i.e., zero uncertainty in the value. In order to accommodate this false assumption, an intended design margin is assigned during analysis to cover the influence of this uncertainty. This margin is called the "factor of safety." The basic fact is that if one has complete knowledge of the events and behavior of the component, there is no need for this margin. It is thus appropriate to term it a "factor of ignorance," where ignorance reflects the lack of knowledge of the uncertainty incorporated in the analysis. Larger safety factors reflect more uncertainty on the part of the designer. By this act, engineers hope to guarantee a safe design. If the margin is set to a high number, it might force an overdesign. The danger is that this approach is not always able to accommodate the lack of knowledge of the uncertainty and it might in some cases result in underdesign. Failures verify this fear where factor of safety did not actually cover the variations in critical parameters.

The premise of classical analysis is that each variable, e.g., force, dimension and material properties contributing to the response of a mechanical system, is single valued. This is almost always far from the truth. A very good treatment of uncertainty is given in Dello (1987) and Dowling (1999). Some pertinent information is taken from these references and this is noted next. The following discussion is influenced by the work cited in the references mentioned above.

For example, every dimension on a drawing has a tolerance band as is every manufactured component. Material properties are based on tests of representative samples. Published values follow statistical protocols. Tensile strength is a value with a mean and standard deviation associated with it developed by the statistical analysis of the data.

It is imperative to incorporate the effect of uncertainty into the design process in a rational manner that is supported by mathematics, physics, and general good sense. In order to do that, the uncertainty must be measured or calculable. The measure of the degree of uncertainty of the likelihood of an event occurring is probability. For many years, it was not possible to perform this analysis. Today, the rapid growth of the availability and capability of computer tools makes this analysis very practical.

A dominant characteristic of engineering design is uncertainty, uncertainty about operational loads, manufacturing dimensions, material properties, etc. Any measured data have uncertainty. The estimation or prediction of the behavior and/or response of a structure based on measured data will also exhibit uncertainty (randomness). There is an assumption of uncertainty in all of these situations. There might also be uncertainty about the validity of a hypothesis or theory that is to be used to predict the performance of the design. The concern is whether or not a model, which was valid in certain circumstances, is applicable to a new situation in which the circumstances are uncertain. Most modeling protocols involve linearization of nonlinear phenomena, e.g., bearing stiffness characteristics used in rotordynamics.

There is a standard joke in process design that "the only place the equipment is not expected to be operated is at the design point!" As engineering knowledge and tools become more sophisticated, the "factor of ignorance" approach will become unsatisfactory. Uncertainty will be applied in the design analysis and decisions will be made based on a calculated response that incorporates the uncertainty in the result.

Siddall (1983) proposed many aspects of utilizing probabilistic based design and provides many reasons to do so. Some of the reasons for adopting probabilistic approaches have been summarized in Siddall (1983):

- Theoretical validity
  - Phenomena encountered in engineering consideration are inherently probabilistic, (i.e., multivalued).
  - Reliability R and failure probability p_f relate directly to performance.
  - Close correspondence between predicted and actual performance requires consideration of variability.
  - Utilization of strength and stress models, which have admissible ranges of values from zero to infinity, takes cognizance of abnormally large stresses and abnormally low strengths that rarely occur.
  - There are functions whose admissible ranges are finite, e.g., the diameter of a shaft, thickness of a shell, etc.
- Reliability
  - An achievable reliability goal should be incorporated into the design methodology with defined levels of performance and defined levels of safety.
- Economic considerations
  - Improved design is expected to minimize costly testing programs for the system.
  - The time from design inception to completion of adequately performing systems will be reduced.
  - Optimized design that meets the reliability and other requirements will have appropriate weight, size volume, etc.
  - A rational approach to costing (total life cost) is needed that includes a policy regarding replacements and warranties.
  - Excess precision and the ability to meet performance requirements will cost more while larger manufacturing tolerances may result in economies.

Application of the Probabilistic Concept

Figure 34 shows a blade from which a test sample is machined. More than one sample is tested to estimate variation in tested properties. The test data will differ depending on the number of samples tested. Some stress-strain curves are shown to depict the possible differences. When the data, e.g., yield strength, ultimate

strength, etc., of the material are plotted as shown, clearly there is a statistical distribution for any property, e.g., yield strength, ultimate strength, etc.

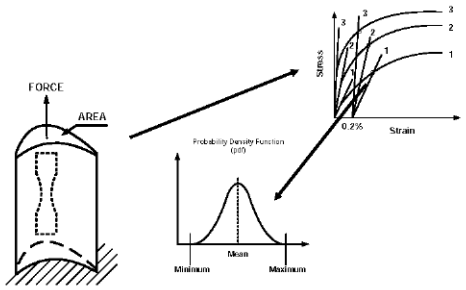

Figure 34. Test Samples of Parts Showing Variability in Data.

Parameters (like loads, material properties, and geometric dimensions) are assumed to be known quantities used with certainty in the deterministic evaluation of the reliability of a mechanical component. The assumption that there is no uncertainty about them is not realistic in any practical application.

Due to uncertainty in the variables, the response (displacement, stress) is also expected to be uncertain. The estimation of the occurrence of a response above the "limit" is a measure of the probability of the risk. Alternatively the number of times a response meets the criteria is a measure of the probability of success, i.e., a measure of the reliability of the structure.

Many probabilistic methods can be employed to estimate reliability, e.g., first order reliability method (FORM) and second order reliability method (SORM). In this particular case, the Monte Carlo simulation method has been used to obtain the solution.

Mathematically, the response of a structure depends on the interaction between the imposed stress (S) and the component's resistance (R). The deterministic method defines the margin by the ratio R/S. There are uncertainties in the values of both S and R and these are represented in statistical terms by a probability density function (PDF). The probability of success is expressed as:

$$P_s = P(R > \text{or} = S) \tag{35}$$

where P_s is the probability of success. In general terms, the above equation takes the following form:

$$P_s = P(H(R,S) > \text{or} = 0) \tag{36}$$

where H(R,S) is a limit function and defines the relationship between R and S. For example, if R is the yield strength of the material and S is the imposed stress, H might be expressed as:

$$H(R,S) = 0.5 * R - S \tag{37}$$

The above relationship states that the limit function, H, is equal to 50 percent of the yield strength less the imposed stress. It is stated that for reliable operation H must be positive, but this is a deterministic statement. The probabilistic aspect of the problem can be stated as follows:

$$P_s = P((0.50*R-S) > \text{or} = 0) \tag{38}$$

A typical representation of the probability density functions for R and S is shown in Figure 35. A vertical line is drawn at the value of 0.50R to represent a limit for the stress magnitude. It can be seen that the average magnitude of S (applied stress) is less than 0.50R (e.g., 50 percent of the yield strength of the material). It satisfies the condition for safe design from a deterministic point of view. However, when consideration is given to the possible uncertainties in R and S, it becomes clear that there is still a possibility of S being larger than R in the area on the middle of the graph where the blue and black curves cross over one another. Hence, there exists a chance of failure due to the statistical nature of R and S but the deterministic approach indicates success.

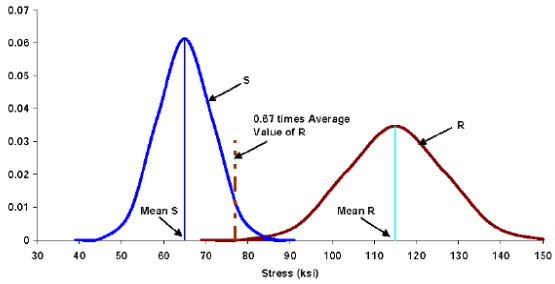

Figure 35. Description of Probability of Failure When ½ the Yield Strength Is Less than or Equal to the Applied Stress.

The following example of a beam under a tensile load demonstrates the importance of the need for probabilistic analysis. A deterministic limit analysis is performed. An assumption is made for the minimum and maximum values of the loads. Also the minimum and maximum possible cross sectional areas of the beam are considered due to the tolerance on the diameter of the beam. The yield strength will have a minimum and maximum value.

$$\text{Factor of safety} = \text{Yield Strength} / (S) \tag{39}$$

where:

S = P/A (P is the applied load and A is the cross sectional area)
Min FS = Minimum value of yield strength/maximum value of S
Max FS = Maximum value of yield strength/minimum value of S
Mean FS = Average value of yield strength/average value of S

The result of the probabilistic analysis (Monte Carlo simulation) that provides the probability of a certain magnitude of FS considering statistical variation of the parameters is shown in Figure 36. Analysis is based on the assumption that material properties and applied load are not single value but these have statistical variations as described earlier in Figure 34. Also the dimension of the cross section of the beam has some tolerances. During manufacturing only thing is guaranteed that the specified dimension stays within the tolerance band. When many beams are manufactured similar way the final dimension will have a statistical dimension even though these are expected to be within the tolerance band. Note that the FS ranges from 1.3 to 1.7.

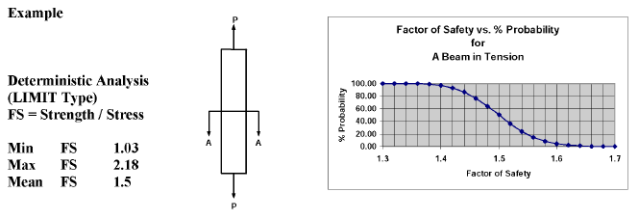

Figure 36. Comparison of Deterministic and Probabilistic Results.

This simple example demonstrates that there is about a 100 percent probability of achieving a factor of safety equal to 1.34 while the probability of achieving a factor of safety of 2.18 (maximum by

limit analysis) is about zero. Of course the probability of achieving the average value of 1.5 is 50 percent, as one should expect.

The probabilistic calculation becomes more complicated, particularly when the response is a function of many variables. To mitigate this complexity, techniques have been developed that perform many calculations (often thousands) rapidly. One such method is Monte Carlo. In Monte Carlo simulation, for example, as the analysis proceeds forward, a picture of the probability of the response being larger than the limit value immerges. The results of Monte Carlo simulations can prove the level of risk associated with the response is larger than the limit value. Based on this information, better decisions can be made regarding the risks of using a component or operating a component with a suspected defect as well as the risks associated with using the component up to a particular number of load cycles.

Probabilistic Treatment of Factor of Safety Based on Goodman's Equation

Singh (2001) has demonstrated the probabilistic reliability assessment of mechanical components. Figure 37 helps explain the reasoning behind this evaluation. It shows an S-N diagram of a material with a band of curves. The band represents the scatter of the test data. The estimated stress applied to a component is also shown to have variation in the y-axis. This variation results from the influence of variations in operating loads, and geometrical tolerances, and also includes the inaccuracy in the estimation procedure.

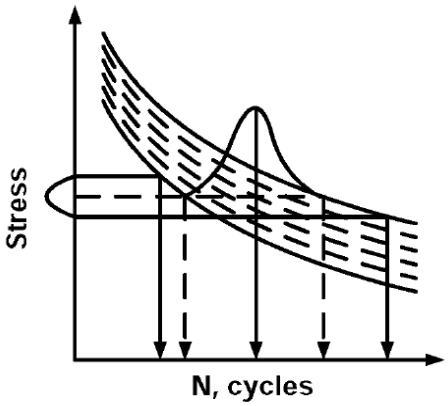

Figure 37. Depicting Scatter of Data in S-n Curve.

The resulting assessment of the operating life is shown on the x-axis. It is clear that due to variations in material property and stress, the operational cycle is not single valued but varies within a range. The implication of this can be seen in the probabilistic Goodman diagram shown in Figure 38. The factor of safety is not single valued but has a range of values; therefore the operating life will also have a range. The band of cycles represents the potential operating life of the blade.

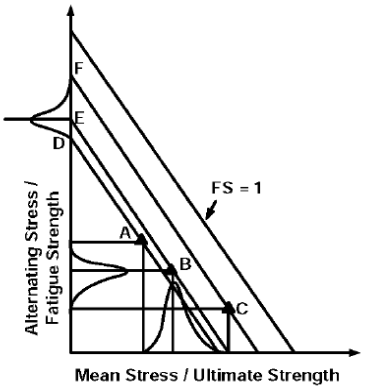

Figure 38. A Probabilistic Aspect of the Goodman Diagram.

The Goodman equation for calculating the factor of safety has been discussed in an earlier section.

Singh (2001) combined this with the life relationship to obtain a relationship for the factor of safety based on life (FN). It is restated below in Equation (40). Both factors of safety, FS and FN, depend on variables such as the mean stress, alternating stress, ultimate strength, fatigue strength and fatigue strength exponent of the material. Uncertainty in the stress due to variations in loading and the observed scatter in the material properties can be described by statistical distributions. After quantifying this uncertainty or scatter in the variables one needs to estimate the chance of the factor of safety (based on stress) having a value larger than a prescribed "limit."

$$FN = ((1 / F.S - \sigma_m / \sigma_{ult}) / ((1 - \sigma_m / \sigma_{ult}))^{(1/b)} \quad (40)$$

The limit function H can be written as:

$$H(FS, \sigma_m, \sigma_{ult}, b) = ((1 / F.S - \sigma_m / \sigma_{ult}) / ((1 - \sigma_m / \sigma_{ult}))^{(1/b)} - FN \quad (41)$$

The probabilistic mathematical statement can be stated as follows:

$$P_s = P(H(FS, \sigma_m, \sigma_{ult}, b) > \text{or} = 0) \quad (42)$$

Example

For demonstration purposes, the following example provides the analytical results for a steam turbine blade:

- Table 3 lists stresses and the calculated factor of safety based on the Goodman equation.

There are two comparable designs for the blades. By examining the magnitude of the calculated FS (last column) it is difficult to identify the better design.

Table 3. Goodman Factor of Safety.

Material: Ti 6Al 4V Solution Treated and aged

Properties:

Ultimate Strength: 179. ksi

Yield Strength: 172. ksi

Fatigue Strength: 60. ksi

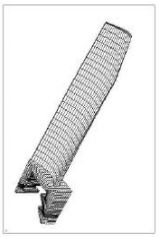

Stress, psi		Factor of Safety
Mean	Alternating	
30,000	20,000	1.996
60,000	10,000	1.993

- The life estimate was made using the same stress magnitude. The estimated lives are listed in the last column of Table 4. The estimated lives show a different picture. Even though the magnitude of life is very large, they are quite different. From this analysis, the difference between the two designs is evident.

Table 4. Life Estimation.

Material: Ti 6Al 4V Solution Treated and aged

Properties:

Ultimate Strength:	179. ksi
Yield Strength:	172. ksi
σ_f'	295.
b	-0.104

Stress, psi		Factor of Safety	Life, Cycles
Mean	Alternating		
30,000	20,000	1.996	2.39E+15
60,000	10,000	1.993	6.30E+19

• The results presented in the above section were obtained using a traditional deterministic type of analysis. Since the stress magnitude and material properties are not single valued, a probabilistic analysis was performed to account for the variability. Table 5 lists the assumed variations of these parameters to be used in the probabilistic analysis.

Table 5. Assumed Variation in Properties (Typical of Turbine Blade Material).

	Total Variations, % of Mean
Ultimate Strength	20
Fatigue Strength	16
Mean Stress	20
Alternating Stress	16
$\sigma f'$	20
b	20

• The blade design was reanalyzed using a probabilistic analysis that incorporated the variations in properties identified in Table 5. The plot in Figure 39 shows the probability versus life cycle for that design evaluation. One can compare that with the deterministic result in Table 5. One observes that there is a considerable deviation between the life in the table versus the range of life on the plot. While the table shows a life of 4.63E+20 cycles, the probabilistic analysis gives a range of life that ranges from 1E+13 to 2.5E+13. These are not even close. Identification of the acceptable level or risk can greatly improve the accuracy of the design life. It also provides more design options. The pink curve depicts reliability and the blue curve shows unreliability.

For the blade

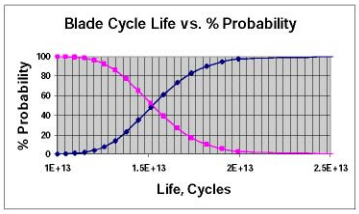

	Stress, psi		FS	Life, cycles
	Mean	Alternating		
Blade	60000	10000	1.993	4.630E+20

Figure 39. Probabilistic Life Assessment for Blade.

Probabilistic Low Cycle Fatigue (lcf) Concept

To account for variability in the material properties, it is practice to test multiple samples. Figure 40 shows results depicting variations in S-N data for the material. It shows that different samples might fail at different numbers of applied cycles even when the applied stress is identical. The strain versus life relationship has been discussed earlier.

$$\Delta\varepsilon_{Total} / 2.0 \quad \text{or strain amplitude, } \varepsilon_{Total} = A\, N_f^b + C\, N_f^d \quad (43)$$

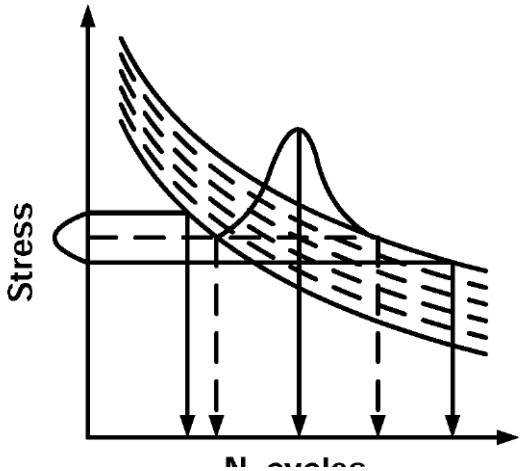

Figure 40. Depicting Scatter of Data in S-N Curve.

The second term is controlled by plastic strains and this strain contributes mainly to lcf type of damage. Even though the total strain should be considered for the estimate, for demonstration purposes the second term will be used to estimate the probabilistic lcf cycles.

$$\varepsilon_{plastic} = C\, N_f^d \quad (44)$$

$$N_f = (\varepsilon_{plastic} / C)^{1/d} \quad (45)$$

The limit function is given by:

$$H(\varepsilon_{plastic}, C, d) = (\boldsymbol{\varepsilon_{plastic}} / C)^{1/d} - \text{cycle} \quad (46)$$

The equation to estimate the probability is given below:

$$P_s = P(H(\varepsilon_{plastic}, C, d) > \text{or} = 0) \quad (47)$$

SUMMARY

It can be stated that the only true certainty in life is that there is uncertainty in life. That is the case in most engineering analyses whether they be quantum physics or turbine blade allowable loading. Thus, no matter what engineering design decisions are made, there is a risk associated with using the calculated results.

In this tutorial, the path followed in the design of turbine blading was discussed. This technology has evolved and grown, driven by needs and technical developments and has been accelerated by the fantastic advances in computers and computational capabilities. As a result, there are much more comprehensive analysis capabilities available today than in past years.

The theory is first explained on the basis of deterministic physics where the basic equations are developed and explained.

Examples of typical results are shown in a stepwise fashion that would be followed in a comprehensive analysis of real turbine blades. However, throughout this analysis, it is assumed that parameters are deterministic, single valued, and constant.

Once this theory is explained, real physics is discussed in which parameters and properties are not single valued or simply deterministic. Rather, all real values have an inherent variability or uncertainty. As a result, solutions are not single valued—rather they are best represented as probabilistic. That is, answers are described as a range with likelihood for each answer. Each value can then be described as having a risk associated with it (likelihood of occurring times cost of occurring). The user can select an answer based on the acceptable level of risk.

It is hoped that the basic theory has been explained in sufficient detail to permit the reader to consider how a "true" analysis must incorporate the uncertainty inherent in any calculation. It is possible to quantify the risk associated with a design analysis. Thus, design decisions do not need to incorporate factors of safety (factors of ignorance) to accommodate the uncertainty. Rather the risk may be quantified and design decisions made on the acceptable level of risk.

One can manage risk when one is able to determine what that risk is. Enhancements in analytical tools and capabilities make that determination a reality. These tools just have to be applied. The authors hope that the users will push for application of the probabilistic analysis tools. They are real but require more application to grow and flourish. The time is right and the needs are there. We are pushing into new frontiers of design from the basis of size, loads, speeds, pressures, materials, costs, and delivery times.

The authors believe that this represents a significant change in demands on design approach. The time has come to integrate the probabilistic analysis into our design tool kit.

LET'S DO IT!!!

REFERENCES

Dello, J., Jan/Feb 1987, "Frequency Evaluation of a Steam Turbine Bladed Disk," *Turbomachinery International*.

Dowling, N. E., 1999, *Mechanical Behavior of Materials,* Upper Saddle River, New Jersey: Prentice Hall.

Drosjack, M., Singh, M., and Rutan, C., 2005, "Determining Risk Associated Inspection and Overhaul of Turbomachinery: Yesterday, Today, and Tomorrow," NPRA, Reliability and Maintenance Conference & Exhibition, New Orleans, Louisiana.

Ewins, D. J., 1969, "The Effects of Detuning upon the Forced Vibrations of Bladed Disk." *Journal of Sound and Vibration, 9,* (1), pp. 65-79.

Griffin, J. H. and Menq, C. H., 1991, "Friction Damping of Circular Motion and Its Application to Vibration Control," ASME *Journal of Vibration and Acoustics, 113,* pp. 225-229.

Menq, C. H., Chidamparam, P., and Griffin, J. H., 1991, "Friction Damping of Two-Dimensional Motion and Its Application in Vibration Control," *Journal of Sound and Vibration, 144,* pp. 427-447.

Sanliturk, K. Y. and Ewins, D. J., 1996. "Modeling Two-Dimensional Friction Contact and Its Application Using Harmonic Balance Method," *Journal of Sound and Vibration, 193,* (2), pp. 511-523.

Siddall, J. N., 1983, *Probabilistic Engineering Design: Principles & Applications,* New York, New York: Marcel Dekker, Inc.

Singh, M. P., 1992, "Predicting the Randomness of Forced Vibration Response of a Bladed Disc," ImechE Conference, Bath, United Kingdom, C432/128.

Singh, M. P., 2001, "Probabilistic HCF Life Estimation of a Mechanical Component," Proceeding of 2001 ASME International Mechanical Engineering Congress and Exposition, New York, New York.

Singh, M., 2006, "Reliability Evaluation of Steam Turbine for Process Drive," A Course Sponsored by Texas A&M University.

Singh, M. P. and Ewins, D. J., 1988, "A Probabilistic Analysis of a Mistuned Bladed Turbine Disc," ImechE Conference, Edinburgh, United Kingdom, C229/88.

Singh, M. P. and Vargo, J. J., 1989, "Reliability Evaluation of Shrouded Blading Using the SAFE Interference Diagram," *Journal of Engineering for Gas Turbine and Power, 111,* pp. 601-609.

Singh, M. and Schiffer, D., 1982, "Vibrational Characteristic of Packeted Bladed Disc," Presented at ASME Design Engineering Technical Conference, Washington, D.C., 82-DET-137.

Singh, M. P., Vargo, J. J., Schiffer, D. M., and Dello, J. D., 1988, "SAFE Diagram—A Design and Reliability Tool for Turbine Blading," *Proceedings of the Seventeenth Turbomachinery Symposium,* Turbomachinery Laboratory, Texas A&M University, College Station, Texas, pp. 93-102.

Srinivasan, A. V., 1997, "Flutter and Resonant Vibration Characteristics of Engine Blades," *Journal of Engineering for Gas Turbines and Power,* Transactions of ASME, *119,* pp. 741-775.

Weaver, F. and Prohl, M., 1956, "High Frequency Vibration of Steam Turbine Buckets," ASME Paper No. 56-A-119.

BIBLIOGRAPHY

Ewins, D. J., 1970, "A Study of Resonance Coincidence in Bladed Discs," *Journal of Mechanical Engineering Science, 12,* (5).

Ewins, D. J., 1973, "Vibrational Characteristics of Bladed Disk Assemblies," *Journal of Mechanical Engineering Science, 15,* (3).

Johnson, D. C. and Bishop, R. E. D., 1956, "The Modes of Vibration of a Certain System Having a Number of Equal Frequencies," *Journal of Applied Mechanics,* Transactions of ASME, pp. 379-384.

Mitchell, M. R., 1978, "Fundamentals of Modern Fatigue Analysis for Design," in Fatigue and Microstructure, ASM International, Materials Park, Ohio, pp. 385-437.

Singh, M. P., 1985, "Turbine Blade Dynamics: A Probabilistic Approach," Vibrations of Blades and Bladed Disk Assemblies, ASME Book No. H000335, pp. 41-48.

Singh, M. P., Thakur, B. K., and Sullivan, W. E., 2005, "Assessing Useful Life of Turbomachinery Components," Proceedings of the Thirty-Fourth Turbomachinery Symposium, Turbomachinery Laboratory, Texas A&M University, College Station, Texas, pp 177-192.